Journal of Nanobiotechnology

RESEARCH

Open Access

NaHS@Cy5@MS@SP nanoparticles improve rheumatoid arthritis by inactivating the Hedgehog signaling pathway through sustained and targeted release of H_2S into the synovium

Xue-Xue Zhu[1†], An-Jing Xu[1†], Wei-Wei Cai[1†], Zhi-Jun Han[2†], Shi-Jie Zhang[1†], Bao Hou[1†], Yuan-Yuan Wen[1], Xing-Yu Cao[1], Hao-Dong Li[1], Yue-Qing Du[1], You-Yi Zhuang[1], Jing Wang[1], Xiao-Ran Hu[1], Xin-Ran Bai[1], Jia-Bao Su[3], Ao-Yuan Zhang[2], Qing-Bo Lu[4], Ye Gu[5*], Li-Ying Qiu[1*], Lin Pan[6*] and Hai-Jian Sun[1,7*]

Abstract

Background Aberrant proliferation and inflammation of fibroblast-like synoviocytes (FLSs) significantly contribute to the pathogenesis of rheumatoid arthritis (RA). Deficiency of hydrogen sulfide (H_2S) is a driving force for the development of RA, and the short half-life of the H_2S-releasing donor sodium hydrosulfide (NaHS) limits its clinical application in RA therapy. Designing a targeted delivery system with slow-release properties for FLSs could offer novel strategies for treating RA.

Methods Herein, we designed a strategy to achieve slow release of H_2S targeted to the synovium, which was accomplished by synthesizing NaHS-CY5@mesoporous silic@LNP targeted peptide Dil (NaHS@Cy5@MS@SP) nanoparticles.

Results Our results demonstrated that NaHS@Cy5@MS@SP effectively targets FLSs, upregulates H_2S and its-producing enzyme cystathionine-γ-lyase (CSE) in the joints of arthritic mice. Overexpression of CSE inhibited the proliferation, migration, and inflammation of FLSs upon lipopolysaccharide (LPS) exposure, effects that were

†Xue-Xue Zhu, An-Jing Xu, Wei-Wei Cai, Zhi-Jun Han and Shi-Jie Zhang and Bao Hou contributed equally to this work.

*Correspondence:
Ye Gu
edwinguye@126.com
Li-Ying Qiu
qiulydoc@sina.com
Lin Pan
linpan0329@163.com
Hai-Jian Sun
sunhaijian927@163.com

Full list of author information is available at the end of the article

mimicked by NaHS@Cy5@MS@SP. In vivo studies showed that NaHS@Cy5@MS@SP achieved a threefold higher AUC_{inf} than that of free NaHS, significantly improving the bioavailability of NaHS. Further, NaHS@Cy5@MS@SP inhibited synovial hyperplasia and reduced bone and cartilage erosion in the DBA/1J mouse model of collagen-induced arthritis (CIA), which was superior to NaHS. RNA sequencing and molecular studies validated that NaHS@Cy5@MS@SP inactivated the Hedgehog signaling pathway in FLSs, as evidenced by reductions in the protein expression of SHH, SMO, GLI1 and phosphorylated p38/MAPK.

Conclusion This study highlights NaHS@Cy5@MS@SP as a promising strategy for the controlled and targeted delivery of H_2S to synoviocytes, offering potential for RA management.

Graphical Abstract

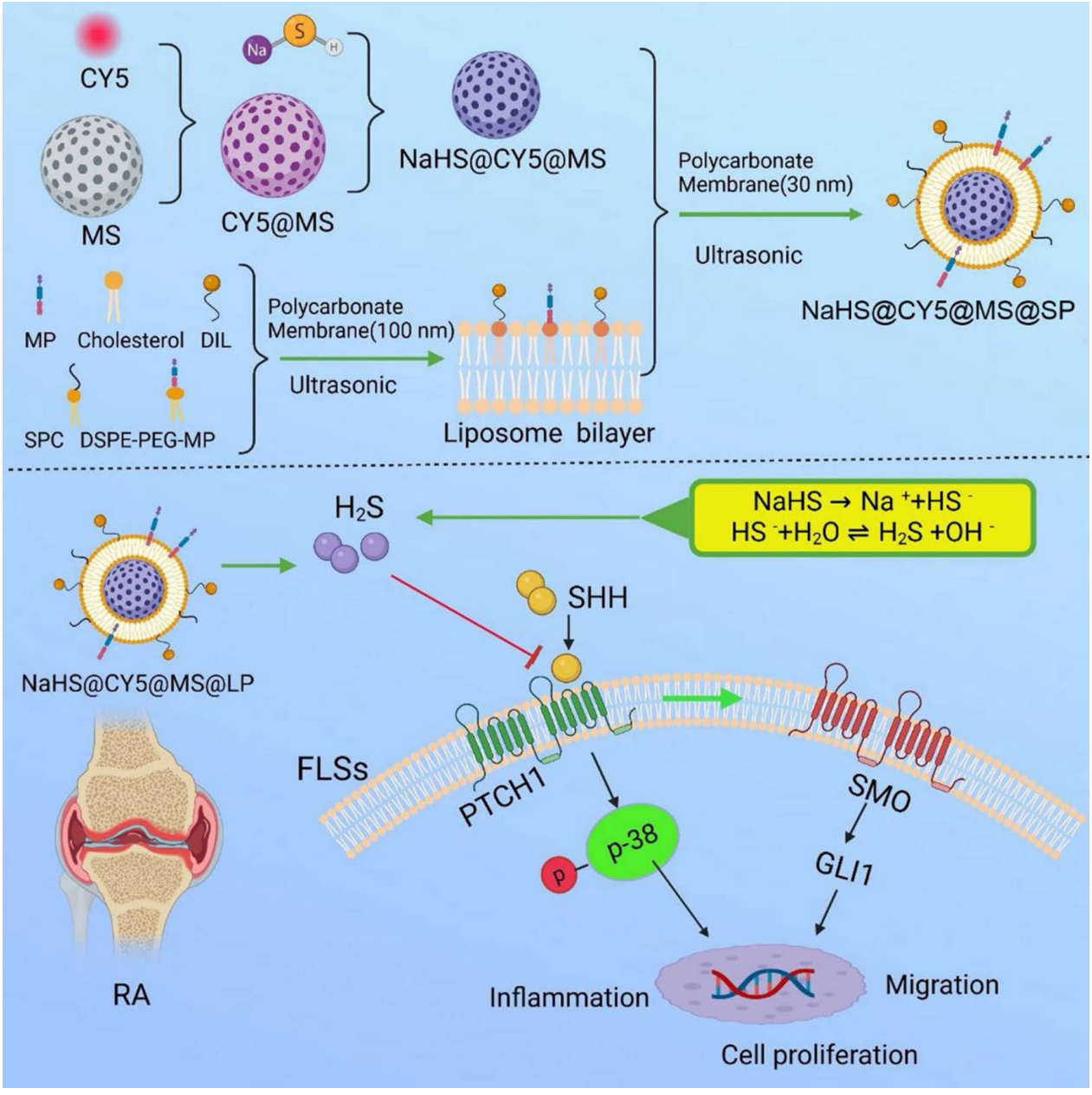

Keywords Rheumatoid arthritis, Fibroblast-like synoviocytes, Hydrogen sulfide, Inflammation, Hedgehog

Introduction

Rheumatoid arthritis (RA) is a chronic inflammatory and autoimmune disorder that usually affects the articular structures and synovial membranes of the joints, leading to local inflammation, joint destruction, remodeling and dysfunctio [1, 2]. To date, RA remains a challenging condition to cure, often requiring lifelong treatment [3]. Current RA therapies include non-steroidal anti-inflammatory drugs (NSAIDs), glucocorticoids (GCs), disease-modifying antirheumatic drugs (DMARDs), and biologic agents. Common examples are ibuprofen (NSAID), dexamethasone (GC), methotrexate (DMARD), and etanercept (biologic agent) [4]. However, the efficacy of such treatments is often limited by several factors, such as poor solubility, low bioavailability, off-target toxicity, and insufficient drug accumulation at inflamed joints [5].

RA is mainly triggered by the activation of fibroblast-like synovial cells (FLSs), leading to the breakdown of the cartilage matrix and destruction of bone [6, 7]. The lining layer of FLSs in the synovium expands significantly from a thickness of 1–3 cells to 10–20 cells, adopting an aggressive phenotype as the disease progresses. The uncontrolled proliferation and migration of aggressive FLSs lead to resistance to cell death signaling in the RA microenvironment [8]. This expansion correlates with disease duration, macrophage infiltration, and the severity of cartilage and bone damage through the production of pathogenic mediators such as inflammatory cytokines, proangiogenic factors, and matrix-degrading enzymes [9]. Targeting FLSs is considered an effective approach to restoring synovial homeostasis and reversing bone and cartilage destruction [6]. The Hedgehog pathway is a critical regulator of embryonic development and tissue homeostasis, and it is activated by three main ligands: Sonic Hedgehog (SHH), Indian Hedgehog (IHH), and Desert Hedgehog (DHH) [10]. Mounting evidence suggests that the Hedgehog signaling pathway plays a significant role in the pathogenesis of RA by regulating synovial inflammation, FLS proliferation, and joint destruction [11]. The activation of Hedgehog signaling promotes hyperproliferation and migration of FLSs, contributing to synovial hyperplasia [12]. Increased expression of SHH, Smoothened (SMO), and GLI family zinc finger 1 (GLI1) has been detected in RA synovial tissue, correlating with disease severity [13, 14]. Given its role in RA progression, targeting the Hedgehog pathway has emerged as a potential therapeutic approach.

Hydrogen sulfide (H_2S), along with nitric oxide (NO) and carbon monoxide (CO), is an endogenous gas that plays a crucial role in regulating inflammatory responses [15–17]. Physiologically, H_2S is produced by the pyridoxal-5′-phosphate-dependent enzymes cystathionine-γ-lyase (CSE), cystathionine-β-synthase (CBS) and 3-mercaptopyruvate sulfurtransferase (3-MST) [18]. CBS is predominantly expressed in the brain, whereas CSE is more highly expressed in the liver, kidneys, and peripheral tissues [18]. Although the exact mechanisms by which H_2S acts as an inflammatory mediator are not fully understood, existing data suggest that it targets multiple and distinct signaling pathways [19]. H_2S levels in plasma and synovial fluid of the knee joint are higher in RA patients compared to healthy controls [20]. The H_2S donor S-propargyl-cysteine (SPRC) has been shown to alleviate adjuvant-induced arthritis in rats by regulating the HDAC6/MyD88/NF-κB signaling pathway [21]. The same group also demonstrated that SPRC displays anti-inflammatory properties in RA by upregulating the Nrf2-antioxidant pathway [22]. H_2S prevents the release of interleukin-6 (IL-6) into FLSs by deactivating the p44/42 mitogen-activated protein kinase [23]. The ability of CSE to reduce the development of RA is attributed to blocking the autoimmune response in FLSs [24]. A novel nano-system, which can simultaneously scavenge NO and release therapeutic H_2S, is reported to mitigate the synovial inflammation, osteoporosis, and clinical symptoms in RA rats [25]. These findings provide solid evidence that H_2S exerted a significant anti-inflammatory effect in the treatment of RA.

The selection of H_2S donors is critical due to the short half-life of this gas in biological fluids and its toxicity at high concentrations. Conventional H_2S donors, such as Na_2S and NaHS, release H_2S rapidly, leading to a significant accumulation of the gas in a short period, which can lead to potential toxicity and reduced treatment efficacy [26]. Therefore, controlled release of H_2S is preferable. One approach is to deliver drugs directly to arthritic joints, ensuring high local concentrations and minimizing off-target effects [27]. The advent of nanomedicine has introduced new avenues for RA treatment. Novel carriers such as liposomes, polymeric nanoparticles, albumin nanoparticles, membrane nanoparticles, dendritic polymers, and gold nanoparticles are being used [28]. Recently, "triggered-release" scaffolds have been reported to enable controlled release and target selectivity of H_2S [29]. While the anti-inflammatory properties of H_2S have been extensively explored, to our knowledge, there are few studies, combining H_2S slow release and synoviocytes-targeting agents in a nano-platform for alleviating RA.

In this study, we developed a novel NaHS@Cy5@MS@SP nanocomplex composed of CY5@SiO2, sodium hydrosulfide (NaHS), SPC, DSPE PEG peptide, cholesterol, and Dil, which can deliver therapeutic H_2S to synoviocytes in a targeted manner. This approach enabled the stable release of H_2S that effectively inhibited the proliferation, migration, and inflammation of FLSs by inactivating the Hedgehog signaling pathway. The H_2S released by NaHS@Cy5@MS@SP had obvious therapeutic

potential in a mouse model of collagen-induced arthritis (CIA). Therefore, it is expected that our proposed administration of H_2S nanomedicine to restrain the proliferation, migration and inflammation of FLSs will delay arthritis progression in RA (Scheme 1).

Materials and methods

Reagents and chemicals

NaHS and lipopolysaccharide (LPS) were bought from Sigma-Aldrich (St. Louis, MO, USA). Trypsin, Dulbecco's Modified Eagle Medium (DMEM), and 1% Penicillin-Streptomycin were procured from Hyclone Laboratories (South Logan, UT, USA). Fetal bovine serum (FBS) was purchased from Boster Biological Technology co. Itd (Wuhan, China). BeyoClick™ EdU Cell Proliferation Kit with Alexa Fluor 488, Western and IP Lysis Buffer, and Proteinase inhibitor were purchased from Beyotime (Shanghai, China). Cell Counting Kit-8 (CCK-8), hochest and DAPI dye was obtained from Biosharp Life Sciences (Beijing, China).

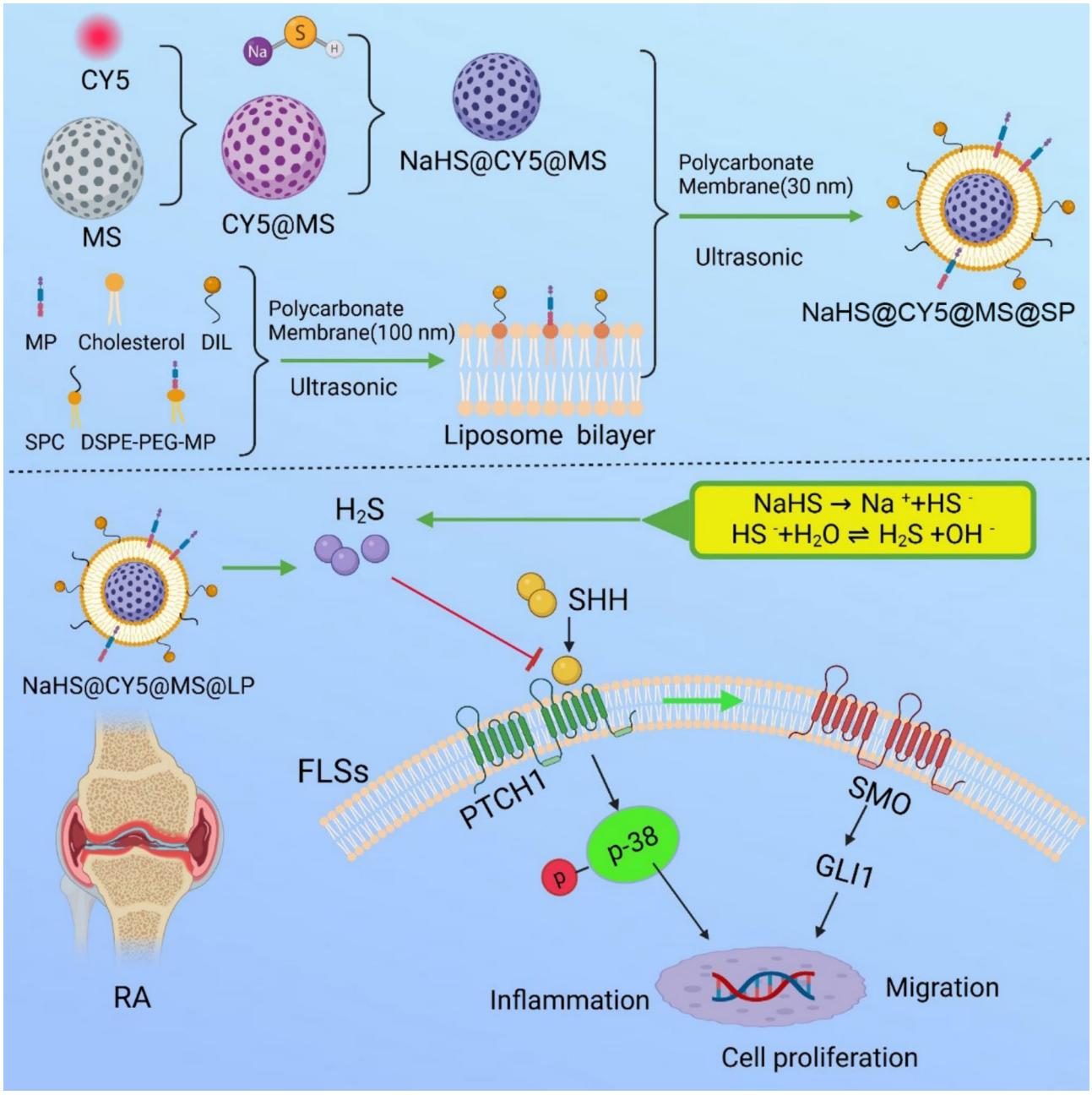

Fig. 1 Preparation of NaHS@Cy5 @ MS@SP nanoparticles and the mechanisms for H_2S in synovium alleviating rheumatoid arthritis via the Hedgehog signaling pathway inhibition and inactivation

Fabrication of NaHS@Cy5@MS@SP nanoparticles

Firstly, mesoporous silicon and CY5 were dissolved in ethanol, stirred at room temperature overnight, centrifuged to remove ethanol, washed in deionized water, and dispersed in deionized water to obtain CY5@SiO2. Then, CY5@SiO2 and sodium hydrosulfide (NaHS) were dissolved in water, stirred at room temperature overnight, centrifuged to remove ethanol, washed in deionized water, and dispersed in deionized water to obtain NaHS@CY5@SiO2. Finally, SPC, DSPE-PEG-polypeptide, cholesterol and DIL were dissolved together in 3 mL of chloroform, evaporated into a film under reduced pressure in sample bottle, supplemented with a small amount of deionized water, sonicated with liposome extruder (polycarbonate film with a pore size of 100 nm), and then sonicated in a water bath for 5 min after adding NaHS@CY5@SiO2. NaHS@Cy5@mesoporous silic@LNP-targeted peptide-DIL (NaHS@Cy5@MS@SP) was obtained by using a nanodialysis device (polycarbonate membrane, pore size 30 nm).

Characterizations of NaHS@Cy5@MS@SP

Dynamic light scattering NanoZS ZEN3600 (Malvern, UK) was used to measure the size and zeta potential of NaHS@Cy5@MS@SP. Fourier transform infrared (FT-IR) spectra (4000–400 cm^{-1}) were recorded by an FT-IR spectrophotometer (Bruker Corporation, FT-IR TENSO-RII, Berlin, Germany). Transmission electron microscopy (TEM, Tokyo, Japan) was used to observe the micromorphology of NaHS@Cy5@MS@SP. Ultraviolet-visible spectrometers (Synergy H4, Bio Tek, America) were used to detect the characteristic groups of NaHS@Cy5@MS@SP.

Animals

Male DBA/1J mice were purchased from GemPharmatech Co., Ltd (Nanjing, China). The animals were housed in the Laboratory Animal Center, School of Medicine, Jiangnan University, at a temperature of 22 ± 2 °C and a humidity of 40–70% with 12-h alternating light and dark. The animal experimental ethics was approved by the Experimental Animal Ethics Committee of Jiangnan University (JN.No20230330d0400930[98]). Forty-five DBA/1J mice were divided into 5 groups with 9 mice in each group, which were divided into control group, model group, Cy5@MS@SP group, NaHS@Cy5@MS@SP group (75 mg/kg), and NaHS group (50 μM/kg), respectively. The doses of NaHS@Cy5@MS@SP and NaHS were selected according to previous reports [21, 25, 30–32]. The control group did not undergo collagen induction treatment, and the other groups underwent collagen induction for a second time 7 days after the first bovine collagen II induction to construct CIA mice. The intervention was administered on day 15, and the blood and internal organs of mice were collected on the 45th day for the detection of relevant indicators. The clinical scoring criteria are: no erythema or swelling, 0 points; Only ankle erythema or mild ankle swelling, 1 point; Ankle joint erythema with mild swelling, 2 points; Ankle to metatarsal joint erythema and moderate swelling, 3 points; Ankle, toe or limb redness and severe swelling, 4 points.

Cellular uptake

RAW264.7 cells and FLSs were cultured in 6 confocal dishes with a density of 1×10^5 cells, and cultured at 37 °C and 5%CO_2 for 6 h. After cell adhesion, the cell media were replaced with 200 μL fresh media containing NaHS@Cy5@MS@SP (0.28 mg/mL). The doses of NaHS@Cy5@MS@SP in cellular experiments were selected according to previous reports [25, 32]. Cells were incubated for 1, 4, and 24 h. Subsequently, cells were fixed with 4% paraformaldehyde for 10 min, washed three times with PBS, stained with DAPI for 10 min, and resuspended in 200 μL PBS. Fluorescence imaging was then performed.

In vivo biodistribution

CIA mice (23–25 g) were randomly divided into 6 groups and administered NaHS@Cy5@MS@SP (75 mg/kg) via tail vein injection. Whole-body fluorescence imaging and ex vivo organ imaging were recorded at 1, 2, 4, 8, 12, and 24 h post-injection using the IVIS spectrum in vivo imaging system under anesthesia at λ_{ex} (650 nm)/λ_{em} (670 nm) (3 mice per time point). All images were analyzed and normalized using Living Imaging software.

Pharmacokinetics analysis

Free NaHS (50 μM/kg) and NaHS@Cy5@MS@SP (75 mg/kg) were injected into CIA mice via the tail vein, and blood samples were collected from the eyeballs at 1, 2, 4, 8, 12, and 24 h after injection (3 mice were taken at each time point). The H_2S content in the blood was then detected using a H_2S assay kit.

Cell culture and treatment

FLSs were maintained in DMEM containing 10% FBS and 1% penicillin/streptomycin (Gibco, Carlsbad, CA, USA) in a 5% CO_2 incubator (HeracellVIOS160i, ThermoScientific, USA) at 37℃. FLS cells were pre-treated with NaHS@Cy5@MS@SP (0.1 mg/mL) and NaHS (100 μM) for 30 min, followed by exposure to LPS (1 μg/mL) for 24 h. To explore the involvement of the Hedgehog signaling pathway, FLS cells were pre-incubated with SAG for 30 min, and then stimulated with LPS (1 μg/mL) for 24 h.

Cell counting kit-8 (CCK-8) assay

FLS cell viability was assessed using CCK-8 assay (Biosharp, Beijing, China). In brief, 10 μL of the CCK-8 reagent was added to each well of a 96-well plate. The plate was then incubated at 37℃ for 1 h. Subsequently, the absorbance at 450 nm was detected by a microplate reader (Winooski, VT, USA).

Micro-CT detection of femur and paw

CIA mice were continuously anesthetized with isoflurane. After anesthesia, the imaging was performed on a small animal imaging bed. Micro-CT (quantum GXII, PE, Germany) was performed to detect the paw deformity, and bone volume fraction (BV/TV) of the femur by analysis 12.0 software. Micro-CT scanning voltage: 90 kv, scanning current: 80 μA, scanning field of view: 86 mm, scanning time: 4 min, scanning mode: high resolution, filter: Cu 0.1 mm, scanning slice thickness: 36 μm.

Masson staining

Firstly, dewaxing was performed on the paraffin sections of the knee joint, followed by gradient hydration. Then, Weigert hematoxylin staining solution was used for staining for 8 min. After washing with water, Masson blue staining solution was used for 5 min, followed by 5 min of Lichun red staining, 1 min of phosphomolybdic acid washing, and 2 min of aniline blue staining. Finally, perform dehydration transparency, film sealing, and microscopic observation.

Safranin fast green staining

After the paraffin section of the knee joint was dewaxed and hydrated, the nucleus was stained with hematoxylin, and then the eosinophilic bone tissue was stained with solid green dye solution for 5 min. After cleaning, the cartilage was stained with safranin dye solution for 5 min. Finally, neutral gum was used to seal and solidify, and then photographed and observed under a microscope.

HE staining

Mice knees were fixed in 4% paraformaldehyde for 10 d, followed by a 4-week decalcification process. The decalcified knees were then embedded in paraffin and cut into 5 μm thick sections. After deparaffinization, the tissue sections were hydrated using gradient ethanol and stained using a hematoxylin-eosin staining kit. The pathological changes of the knee joint were observed using a digital slice scanner (3DHISTECH, Hungary).

Immunohistochemical (IHC) staining

IHC staining of IL-6 and TNF-α in the knee joint of rats was performed. The knee joint was first dewaxed, followed by gradient alcohol hydration, citric acid antigen repair, peroxidase inactivation, and BSA closure. Subsequently, the slices were incubated with specific primary antibodies (dilution 1:200) at 4 °C overnight. On the second day, the tissue sections were rewarmed at 37 °C for 1 h, washed with PBS buffer solution, and then stained with horseradish peroxidase (HRP) labeled secondary antibody at room temperature for 2 h. Finally, a digital slide scanner (3DHISTECH, Hungary) was used to observe the expression of inflammatory factors in the knee joint of rats.

5-ethynyl-2′-deoxyuridine (EdU) staining

The detection of cell proliferation was used BeyoClick™ EdU Cell Proliferation Kit with Alexa Fluor 488 (Beyotime, Shanghai, China). Briefly, the treated FLS cells were fixed with 4% paraformaldehyde (Solarbio, Beijing) for 1 h. Following washing three times, cells were pretreated with 0.5% TritonX-100 for 15 min, and then incubated with 50 mM EdU for 2 h under ambient environment. The nuclei were dyed with Hoechst 33,342 and imaged with a ZEISS fluorescence microscope (Zeiss Axio imagar 2, Germany).

Cell migration assay

To assess the migration and invasion ability of FLS cells, serum-free DMEM was added to the upper chamber, while 750 μL medium containing 10% FBS was added to the lower chamber. After stimulation for 24 h, FLS cells on the upper surface of the transwell filters were wiped with a cotton swab. The migrated cells were stained with 1% crystal violet. The images were observed and photographed under a microscope (Nikon, Japan).

Immunofluorescence staining

The joint sections underwent fixation, paraffin embedding, deparaffinization, hydration, and heat-induced antigen retrieval. The FLS cells were fixed with 4% paraformaldehyde at 4℃ for 1 h. After washing with PBS three times, the samples were permeabilized by 0.1% Triton X-100 for 15 min, and subsequently blocked by 5% BSA at 37℃ for 1 h. After three PBS washes, the samples were incubated overnight with the indicated antibody at 4℃. On the next day, samples were stained with fluorescently labeled secondary antibodies (Invitrogen) at 37℃ for 1 h under light-protected environment. The nuclei were visualized with 4′,6-diamidino-2-phenylindole (DAPI). The images were observed and captured using a ZEISS fluorescence microscope (Zeiss Axio imagar 2, Germany).

Enzyme-linked immunosorbent assay (ELISA)

The levels of tumor necrosis factor-α (TNF-α), interleukin-6 (IL-6) and vascular endothelial growth factor (VEGF) were determined by ELISA kits (Elabscience, Wuhan, China) under the guideline of manufacturer's

protocols. The absorbance values were read using a microplate instrument (Synergy H4, BioTek, Winooski, VT, USA) at 450 nm.

Western blotting

After samples were lysed by Ultrasonic Cell Crusher (Xinchen, Nanjing, China), total protein concentrations were measured by BCA Protein Quantification Kit (Abbkine, Wuhan, China). An equal quantity of protein underwent sodium dodecyl sulfate-polyacrylamide gel (SDS-PAGE) and was subsequently transferred onto the polyvinylidene difluoride (PVDF, Millipore Darmstadt, Germany) membrane. After that, the membranes were blocked by 5% skim milk (Beyotime, Shanghai, China), followed by incubated with the indicated primary antibodies overnight at 4℃. After washing with TBST, the blots were exposed to horseradish peroxidase (HRP)-coupled secondary antibodies at room temperature for an hour. The following antibodies were used in this study: anti-CSE (60234-1-Ig, Proteintech), anti-CBS (67861-1-Ig, Proteintech), anti-3-MST (ab96705, Abcam), anti-SHH (20697-1-AP, Proteintech), anti-SMO (20787-1-AP, Proteintech), anti-GLI1 (66905-1-Ig, Proteintech), anti-P-P38 (9211, Cell signaling), anti-T-P38 (9212, cell signaling technology) and anti-β-actin (66009-1-Ig, Proteintech), HRP-linked anti-rabbit IgG (SA00001-2, Proteintech), HRP-linked anti-mouse IgG (SA00001-1, Proteintech). Eventually, the blots were visualized using enhanced chemiluminescence solution (ECL, Biosharp, Shanghai, China). ImageJ software (version 1.53t) was applied to analyze the densities.

Reverse transcription-polymerase chain reaction (RT-PCR)

Total RNA from FLS cells was extracted using TRIzol Reagent (Vazyme BioTech Co., Ltd, Nanjing) according to the manufacturer's instructions. RNA concentration and purity were measured using ultramicro spectrophotometer (Nanodrop one, Thermo Fisher Scientific, USA). RNA (1 μg) of each sample was subjected to reverse-transcription with Hifair® AdvanceFast 1st Strand cDNA Synthesis Kit (Yeasen, Shanghai, China). Real-time PCR was carried out using Hieff® qPCR SYBR® Green Master Mix (Yeasen Biotechnology, Shanghai, China) under the LightCycler 480 II PCR System (Roche, USA). The relative expression levels of indicated genes were normalized to β-actin and calculated using $2^{-\triangle\triangle Ct}$ method. Gene-specific primers were shown in Table 1.

Table 1 The primer sequences used in this study

Target gene	Primer sequences (5'-3')
CSE	Forward: CATGAGTTGGTGAAGCGTCAG Reverse: AGCTCTCGGCCAGAGTAAATA
CBS	Forward: GGCCAAGTGTGAGTTCTTCAA Reverse: GGCTCGATAATCGTGTCCCC
3-MST	Forward: TGCTGGCTTTGGACCAGAATA Reverse: GCAAACCAGTCAATGCACTGA
IL-6	Forward: CCTGAACCTTCCAAAGATGGC Reverse: TTCACCAGGCAAGTCTCCTCA
COX2	Forward: TCCACAGTTACCCGGAGTTTA Reverse: GCCGAGCTATCAACCGGAT
MMP-1	Forward: AAAATTACACGCCAGATTTGCC Reverse: GGTGTGACATTACTCCAGAGTTG
MMP-3	Forward: CTGGACTCCGACACTCTGGA Reverse: CAGGAAAGGTTCTGAAGTGACC
MMP-9	Forward: TGTACCGCTATGGTTACACTCG Reverse: GGCAGGGACAGTTGCTTCT
β-actin	Forward: CCGAGCCGTGTTTCCTTCC Reverse: GCCATGCTCAATGGGGTACT

Transcriptome sequencing analysis

Transcriptome sequencing and analysis were carried out by OE Biotech Co., Ltd. (Shanghai, China), as previously reported [16, 33, 34]. In brief, total RNA in each sample was extracted using TRIzol reagent (Invitrogen, CA, USA) according to the manufacturer's protocols. RNA purity and concentration were assessed with a NanoDrop 2000 spectrophotometer (Thermo Scientific, USA), while RNA integrity was evaluated using the Agilent 2100 Bioanalyzer (Agilent Technologies, Santa Clara, CA, USA). RNA libraries were prepared using the VAHTS Universal V6 RNA-seq Library Prep Kit following the manufacturer's instructions. Transcriptome sequencing and subsequent analysis were performed by OE Biotech Co., Ltd. (Shanghai, China), with sequencing carried out on the Illumina NovaSeq 6000 platform using 150 bp paired-end reads. The raw reads per sample were generated. Raw reads in fastq format were processed with fastp1, and low-quality reads were removed to yield clean reads. After filtering, the clean reads per sample were retained for further analysis. Clean reads were aligned to the reference genome using HISAT22. Gene expression was quantified by calculating FPKM values for each gene, and gene read counts were obtained using HTSeq-count4. Principal component analysis (PCA) was performed in R (v 3.2.0) to evaluate sample duplication and biological variability. Differential expression analysis was conducted using DESeq25, with a threshold set at Q value < 0.05 and fold change > 2 or < 0.5 to identify significantly differentially expressed genes (DEGs). Hierarchical clustering of DEGs was performed in R to visualize gene expression patterns across different groups and samples. A radar plot of the top 30 up- and down-regulated DEGs was generated using the gradar package in R. Enrichment analysis of DEGs was conducted for Gene Ontology (GO), KEGG pathways, Reactome, and WikiPathways using hypergeometric distribution, all performed in R (v 3.2.0). The raw RNA sequencing data in this study is deposited in the public database (the Sequence Read Archive, SRA) under accession number PRJNA1143598.

Statistical analysis

All values were represented as mean ± SEM. All cell experiments were repeated 4–6 times, and animal experiments were repeated 5–6 times, except for the transcriptome which had 3 samples per group. All data were analyzed with GraphPad Prism software. Differences between two groups were performed using unpaired t-test. Comparisons between multiple groups were analyzed using ANOVA followed by the Bonferroni post hoc test, with $p < 0.05$ considered significant.

Results and discussion

CSE decreased the inflammatory response in LPS-induced FLS cells

To investigate the role of endogenous H_2S in LPS-evoked inflammation within the context of RA, we focused on the three key enzymes responsible for H_2S generation, including CSE, CBS, and 3-MST, in FLSs. Notably, only the protein expressions and mRNA levels of CSE, and not those of CBS or 3-MST, were significantly enhanced in LPS-exposed FLSs (Fig. 2A-B). Immunofluorescence (IF) staining further confirmed the upregulated expression of CSE in LPS-induced FLSs and joint tissue of arthritic mice (Fig. 2C). This was paralleled by an increase in H_2S content in response to LPS, indicating a compensatory upregulation of CSE enzyme and H_2S production in both LPS-induced FLSs and synovial tissue of RA mice (Fig. 2D). The significant upregulation of CSE in response to LPS suggests a compensatory mechanism aimed at counteracting inflammation through increased H_2S production. Previous studies have established that H_2S possesses anti-inflammatory properties [35–37], and our data corroborate these findings by demonstrating that overexpression of CSE, and consequently H_2S, can ameliorate LPS-induced inflammatory responses in FLS cells.

To assess the impact of CSE on inflammation related to RA pathogenesis, FLSs were transfected with a CSE overexpression plasmid. Overexpression of CSE notably increased the protein and mRNA levels of CSE in FLS cells (Fig. 2E-F). This overexpression ameliorated LPS-induced inflammatory responses, as evidenced by the downregulation of mRNA levels of interleukin-6 (*IL-6*) and cyclooxygenase-2 (*COX-2*), along with a reduction in the release of tumor necrosis factor α (TNF-α) and IL-6, as determined by RT-PCR and ELISA analysis (Fig. 2G-J). Furthermore, both the CCK-8 assay and EdU staining indicated that CSE overexpression inhibited LPS-stimulated synoviocyte viability (Fig. 2K-L). Importantly, LPS-induced migration of FLS was prevented by CSE overexpression (Fig. 2M). Additionally, LPS increased vascular endothelial growth factor (VEGF) release and elevated the mRNA levels of matrix metalloproteinase (*MMP*)*-1*, *3*, and *9*, effects which were reversed by CSE overexpression (Fig. 2N-O). These findings highlight the pivotal role of CSE and the endogenous production of H_2S in modulating inflammatory responses in RA. The observed reduction in *IL-6* and *COX-2* mRNA levels, as well as the decreased release of TNF-α and IL-6 upon CSE overexpression, underscores the anti-inflammatory potential of CSE-derived H_2S. These cytokines are well-known mediators of inflammation and are critically involved in the pathogenesis of RA. Therefore, targeting CSE to boost H_2S production could represent a novel therapeutic strategy for mitigating inflammation in RA. This study identifies CSE and the H_2S pathway as critical modulators of inflammation in RA, offering new insights into the potential therapeutic applications of targeting CSE for RA treatment.

Fabrication and characterization of NaHS@Cy5@MS@SP nanoparticles

Mesoporous silicon is widely used due to its high loading capacity and excellent biocompatibility [38]. Additionally, targeted peptide fusion liposomes efficiently deliver drugs to target cells [39]. In this study, mesoporous silicon loaded with NaHS was prepared, followed by the creation of a fusion liposome membrane targeting fibroblast synovial cells through sonication and liposome extrusion. Finally, a nano-dialysis device was employed to encapsulate the liposome membrane on mesoporous silicon, resulting in NaHS@Cy5@MS@SP (Fig. 3A). Transmission electron microscopy revealed that MS and NaHS@Cy5@MS@SP had a spherical structure (Fig. 3B-C), and the surface of the NaHS@Cy5@MS@SP nanoparticles can be seen to be coated with a milky white liposome. The ZetaPALS analyzer measured the hydrodynamic size of MS and NaHS@Cy5@MS@SP were 60.58 ± 2.16 nm and 130.23 ± 4.36 nm respectively (Fig. 3D-E). The zeta potential of MS and NaHS@Cy5@MS@SP were − 0.51 ± 0.012 mV and − 15.24 ± 2.04 mV, respectively (Fig. 3F). The PDI of MS and NaHS@Cy5@MS@SP were 0.153 ± 0.01 and 0.163 ± 0.01, respectively (Fig. 3G). The loading rate of NaHS@Cy5@MS@SP for both Cy5 and NaHS was approximately 4.2% (Fig. 3H), and the encapsulation rate was close to 90% (Fig. 3I). The stability test results show that the particle size of NaHS@Cy5@MS@SP has no significant change in the pH range of 5–9, but the potential fluctuates between − 6 mV and − 15 mV, and the lowest potential is close to -15 mV at pH = 7 (Fig. 3J-K). When the temperature increased from 25 °C to 37 °C, the particle size expanded from 130 nm to about 140 nm, and the potential fluctuated between − 6mV and − 17 mV (Fig. 3L-M).

UV-vis spectroscopy results showed no significant change in the absorption peak position of NaHS@Cy5@MS@SP after loading NaHS, but the absorption intensity increased significantly, likely due to the $n \rightarrow \sigma^*$ transition of the -S group [40], particularly around the wavelength

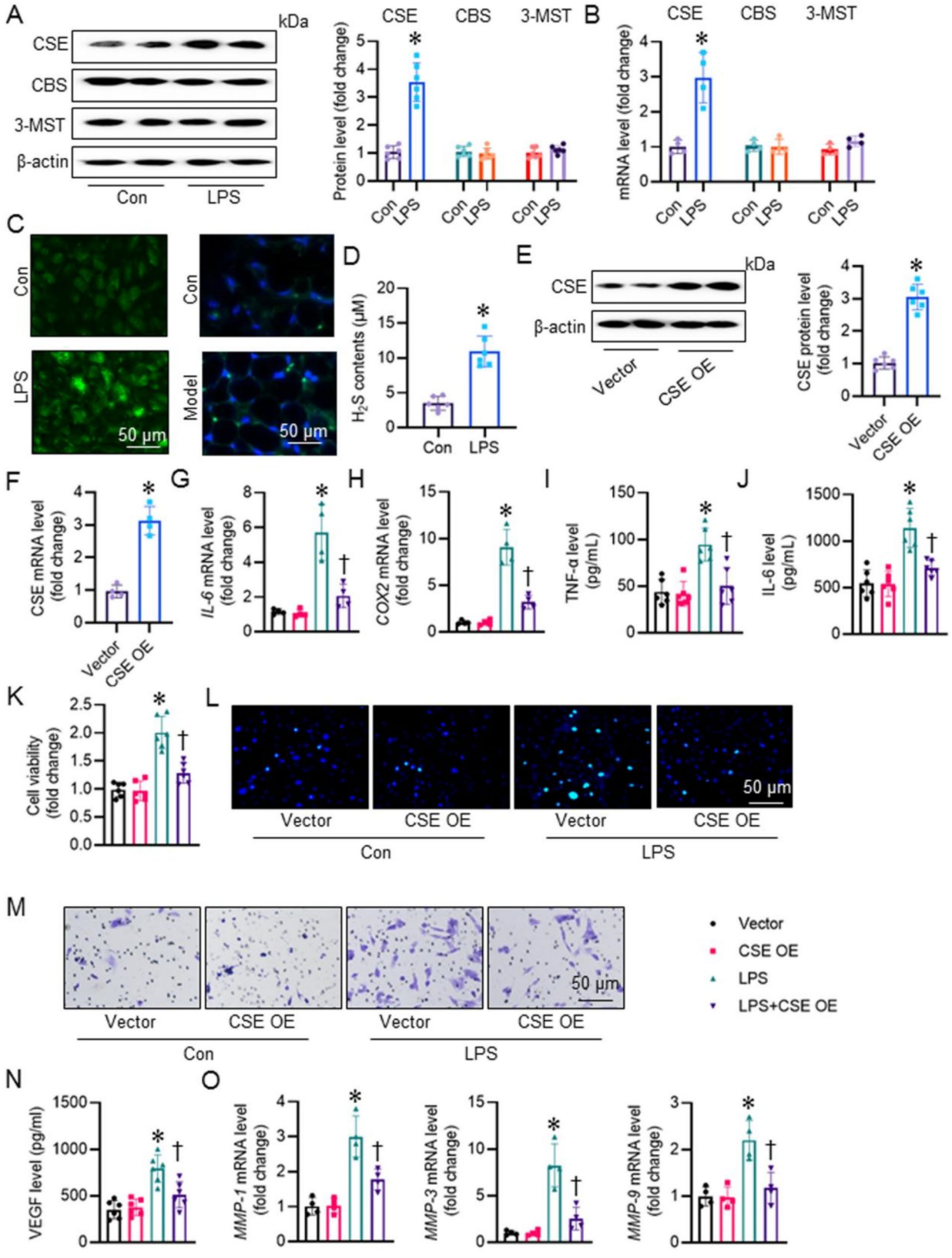

Fig. 2 (See legend on next page.)

(See figure on previous page.)

Fig. 2 CSE inhibited FLS cells inflammation and growth in vitro. (**A**) Western blot analysis of CSE, CBS and 3-MST protein levels in FLSs treated with LPS. (**B**) RT-PCR analysis of CSE, CBS and 3-MST mRNA levels in FLSs treated with LPS. (**C**) Immunofluorescence analysis of CSE in FLSs treated with LPS and joint tissue of RA mice. (**D**) H_2S levels in FLSs treated with LPS. (**E**) Western blot analysis of CSE protein levels in FLSs. (**F**) RT-PCR analysis of CSE in FLSs. (**G-H**) RT-PCR analysis of *IL-6* and *COX2*. (**I-J**) The levels of TNF-α and IL-6 measured by ELISA. (**K**) Cell viability. (**L**) Representative photographs of EdU-positive cells. (**M**) Transwell migration assay. (**N**) The level of VEGF. (**O**) RT-PCR analysis of *MMP-1*, *MMP-3*, and *MMP-9*. *P < 0.05 versus Con or Vector; †P < 0.05 versus LPS. n = 4–6. H_2S, hydrogen sulfide; CSE, cystathionine-γ-lyase; CBS, cystathionine-β-synthase; 3-MST, 3-mercaptopyruvate sulfurtransferase; FLSs, fibroblast-like synoviocytes; LPS, lipopolysaccharide; RT-PCR, Reverse transcription-polymerase chain reaction; IL-6, interleukin-6; COX2, cyclooxygenase-2; TNF-α, tumor necrosis factor-α; EdU, 5-Ethynyl-2′-deoxyuridine; VEGF, endothelial growth factor; MMP-1, matrix metalloproteinase-1; MMP-3, matrix metalloproteinase-3; MMP-9, matrix metalloproteinase-9

of 200 nm (Fig. 3N). The IR spectrum indicated a significantly enhanced absorption band in the range of 2857–3000 cm^{-1} for the NaHS@Cy5@MS@SP group compared to the Cy5@MS@SP group (Fig. 3O), which may be attributed to the presence of the S-H bond in NaHS [41]. The absorption band at 1091 cm^{-1} is the vibrational absorption band of the Si-O bond. Both UV-vis and IR spectra confirmed the successful encapsulation of NaHS in NaHS@Cy5@MS@SP.

Cellular uptake of NaHS@Cy5@MS@SP

To investigate intracellular localization and uptake pathways, the hydrophilic dye Cy5 was encapsulated within the nucleus of mesoporous silicon, while the lipophilic dye DIL was incorporated into the liposome lobules. DIL, being hydrophobic, localizes in the lipid bilayer of the cell membrane during NaHS@Cy5@MS@SP uptake, whereas Cy5 is endocytosed into the cytoplasm. Confocal microscopy was employed to observe the uptake of NaHS@Cy5@MS@SP by cells.RAW264.7 macrophages were selected to study the uptake process over 24 h, given their phagocytic capabilities. After incubating NaHS@Cy5@MS@SP with RAW264.7 cells for 1 h, significant red fluorescence from Cy5 was detected in the cells, while the orange fluorescence from DIL was weak. The red fluorescence remained concentrated in the cytoplasm and did not vary significantly over time. In contrast, the orange fluorescence gradually increased and was localized on the cell membrane (Fig. 4A). For targeted delivery to joint cells, FLS targeting peptides were incorporated into the NaHS@Cy5@MS@SP liposomal shell. FLS cells were used to evaluate the uptake of NaHS@Cy5@MS@SP (Fig. 4B). After co-incubation with FLS cells for 1 h, strong red fluorescence from CY5 was observed in the cytoplasm, while the orange fluorescence from DIL was relatively dim. After 4 h, the orange fluorescence on the cell membrane significantly increased, and after 24 h, the intensity of orange fluorescence on the FLS cell membrane was approximately twice that observed in RAW264.7 cells (Fig. 4C-D). These results indicate that NaHS@Cy5@MS@SP exhibits effective targeting of FLS cells, likely due to the presence of FLS targeting peptides.

In vivo distribution of NaHS@Cy5@MS@SP

To evaluate the targeted delivery of NaHS@Cy5@MS@SP to joint synovium in vivo, we assessed its biodistribution in CIA mice. NaHS@Cy5@MS@SP was administered via tail vein injection, and its accumulation in the joints was monitored over a 24-h period. Red fluorescence from Cy5 in the feet of CIA mice increased gradually from 1 to 24 h post-injection, indicating progressive accumulation of NaHS@Cy5@MS@SP in the joint synovium (Fig. 5A). Dissection and live imaging of the mice revealed that, over time, NaHS@Cy5@MS@SP primarily accumulated in the liver for metabolism and showed minimal presence in other organs (Fig. 5B). This demonstrates the targeted delivery of NaHS@Cy5@MS@SP to the synovial membrane of the joints.

In addition, in vivo pharmacokinetics of NaHS and NaHS@Cy5@MS@SP were studied in mice following a single intravenous administration (Fig. 5C-D). The results demonstrated that NaHS was rapidly degraded in blood circulation, with a half-life ($t_{1/2}$) of 4.51 ± 0.3 h. In contrast, the release of NaHS from NaHS@Cy5@MS@SP was significantly prolonged, with a $t_{1/2}$ of 17.07 ± 1.2 h. The maximum concentration (C_{max}) of NaHS was 164.78 nmol/mL, while NaHS in the NaHS@Cy5@MS@SP group reached a Cmax of 181.53 nmol/mL. Additionally, the area under the curve (AUC_{inf}) for NaHS@Cy5@MS@SP was three times higher than that of free NaHS, indicating significantly improved bioavailability. These findings suggest that NaHS encapsulated in NaHS@Cy5@MS@SP can circulate in the blood for an extended period, maintain a higher blood drug concentration, and is more likely to accumulate at the target site to exert its therapeutic effect.

Therapeutic effect of NaHS@Cy5@MS@SP on CIA mice

The experiment design for the animal study was shown in Fig. 6A. NaHS@Cy5@MS@SP was administered via tail vein to CIA mice, and its therapeutic potential for RA was evaluated after 30 days of intervention. As shown in Fig. 6B, NaHS@Cy5@MS@SP significantly reduced ankle swelling in CIA mice, with a swelling inhibition rate of (50 ± 4.16%) compared to the model group. Micro-CT

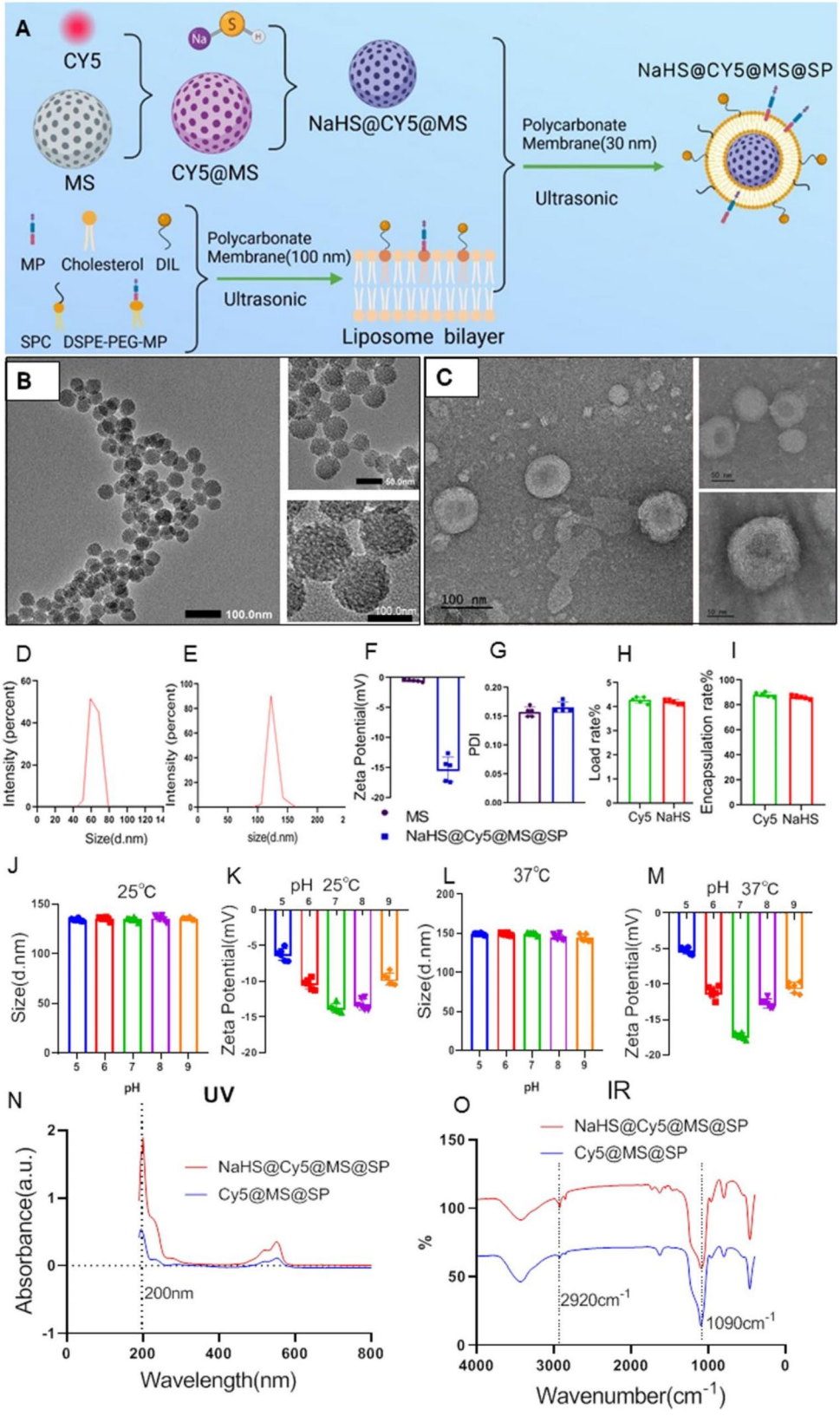

Fig. 3 (See legend on next page.)

(See figure on previous page.)

Fig. 3 Preparation and characterization of NaHS@Cy5@MS@SP nanoparticles. (**A**) Preparation of NaHS@Cy5@MS@SP Nanoparticles. (**B** and **C**) Transmission electron microscope images of MS and NaHS@Cy5@MS@SP. (**D** and **E**) Size of MS and NaHS@Cy5@MS@SP. (**F**) Zeta potential of MS and NaHS@Cy5@MS@SP. (**G**) PDI of MS and NaHS@Cy5 @ MS@SP. (**H** and **I**) NaHS@Cy5@MS@SP Loading capacity and encapsulation efficiency for NaHS and Cy5.(**J-M**) Particle size and potential of NaHS@Cy5@MS@SP in the pH range of 5–9 at 25 °C and 37 °C. (**N**) UV spectrogram of NaHS@Cy5@MS@SP and Cy5@MS@SP. (**O**) IR spectrogram of NaHS@Cy5@MS@SP and Cy5@MS@SP. MS, Mesoporous silicon; DIL, 1,1′-dioctadecyl-3,3,3′,3′-tetramethylindocarbocyanine perchlorate; SPC, Soy lecithin; DSPE-PEG-MP, 1, 2-distearoyl-Sn-glycerol-3-phosphate ethanolamine-Polyethylene glycol-polypeptide; SP, Soy lecithin bimolecular polypeptide; NaHS, Sodium Hydrosulfide; UV, Ultra Violet; IR, Infrared ray

imaging, known for its precise qualitative and quantitative assessment capabilities [42, 43], demonstrated substantial improvements in ankle bone deformity in both NaHS@Cy5@MS@SP and NaHS groups (Fig. 6C). Additionally, Micro-CT imaging of the entire foot revealed significant improvements in foot joint enlargement in CIA mice treated with NaHS@Cy5@MS@SP (Fig. 6D). The red arrow points to the joint deformity site. The clinical score of arthritis severity shows that both NaHS@Cy5@MS@SP and NaHS have significant improvement effects on arthritis (Fig. 6E). Analysis using Analyze 12.0 indicated that NaHS@Cy5@MS@SP significantly enhanced the bone volume fraction (BV/TV%), bone surface area to tissue volume ratio (BS/TV%), and bone surface area to bone volume ratio (BS/BV) in CIA mice, outperforming the NaHS intervention group (Fig. 6F-H). Although there was no significant difference in the cortical bone thickness of the ankle among the groups (Fig. 6I), the model group exhibited a significant reduction in trabecular number, which was reversed by NaHS@Cy5@MS@SP intervention (Fig. 6J). Furthermore, trabecular thickness analysis showed superior results in the NaHS@Cy5@MS@SP group compared to the NaHS group (Fig. 6K). These results indicate that NaHS@Cy5@MS@SP not only reduces foot swelling and bone mineral density loss in CIA mice, but also has a protective effect on the ankle joint.

Pathological evaluation of the joint after NaHS@Cy5@MS@SP intervention

Partial knee lesions are a hallmark of RA [44, 45]. The therapeutic efficacy of NaHS@Cy5@MS@SP on knee joint pathology was assessed through various staining methods. Masson's staining revealed collagen fibers in blue, which are typically abundant during bone injury repair [46]. As illustrated in Fig. 7A, extensive blue staining was observed at the cartilage repair sites in the control, NaHS@Cy5@MS@SP, and NaHS groups, indicating substantial collagen presence. In contrast, the model and Cy5@MS@SP groups exhibited reduced collagen fiber expression. Hematoxylin and eosin (HE) staining in the model and NaHS@Cy5@MS@SP groups revealed prominent inflammatory factors and inflammatory pannus (Fig. 7B). Safranin and fast green staining demonstrated that knee cartilage (indicated by blue arrows) was thinner and more severely damaged in the model and NaHS@Cy5@MS@SP groups. However, cartilage recovery was notably better in the NaHS@Cy5@MS@SP intervention group (Fig. 7C). Immunohistochemical (IHC) staining for inflammatory markers IL-6 and TNF-α showed significantly elevated levels in the model group compared to the control group. This elevation was effectively reversed following NaHS@Cy5@MS@SP treatment (Fig. 7D-E, H-I).

Additionally, immunofluorescence staining for macrophage markers CD206 and CD86 indicated that the model group had lower CD206 expression and higher CD86 expression, reflecting a predominance of pro-inflammatory M1 macrophages. Conversely, the NaHS@Cy5@MS@SP intervention group exhibited higher CD206 expression and lower CD86 expression compared to the NaHS group, suggesting a shift towards anti-inflammatory M2 macrophages (Fig. 7F-G, J-K). In summary, pathological staining results demonstrate that both NaHS@Cy5@MS@SP and NaHS treatments can alleviate knee joint lesions, with NaHS@Cy5@MS@SP showing more pronounced therapeutic benefits.

NaHS@Cy5@MS@SP decreased pro-inflammatory expression in LPS-provoked FLSs

In order to elucidate the impact of NaHS@Cy5@MS@SP on pro-inflammatory expression in LPS-provoked FLSs, various concentrations of NaHS@Cy5@MS@SP were administered to FLSs. Our experiments demonstrated that NaHS@Cy5@MS@SP did not significantly affect cell viability (Fig. 8A), but it did enhance the mRNA levels of cystathionine-γ-lyase (CSE) within the concentration range of 0.05-1 mg/mL (Fig. 8B). Upon LPS exposure, the release of TNF-α was markedly increased; however, treatment with NaHS@Cy5@MS@SP (0.05-1 mg/mL) effectively inhibited this response (Fig. 8C). Consequently, the dose of 0.1 mg/mL was selected for subsequent cellular experiments. The lack of impact on cell viability suggests that NaHS@Cy5@MS@SP is non-toxic at the tested concentrations, making it a promising therapeutic candidate. The upregulation of CSE mRNA levels by NaHS@Cy5@MS@SP indicates a potential mechanism through which H_2S-mediated anti-inflammatory effects are enhanced. This is particularly relevant as CSE is a key enzyme in H_2S biosynthesis, and H_2S has been shown to possess anti-inflammatory properties.

IL-6 and COX-2 are pivotal mediators in the inflammatory cascade associated with RA, and their downregulation is indicative of a significant anti-inflammatory effect. Further analysis revealed that both NaHS@Cy5@MS@SP

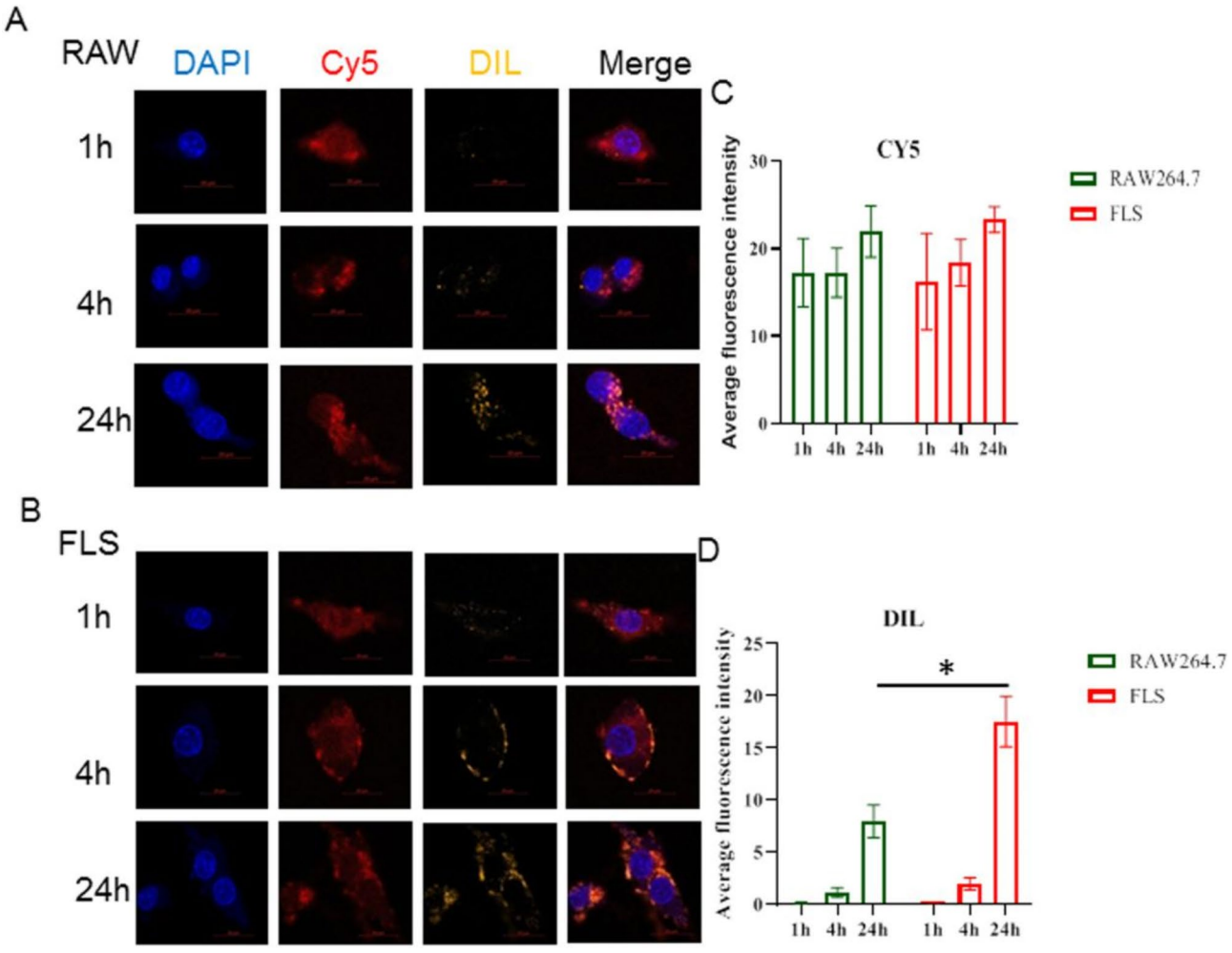

Fig. 4 In vitro cellular uptake of NaHS@Cy5@MS@SP. After co-culture for 1 h, 4 h and 24 h respectively, images were captured using Zeiss confocal microscope to observe the uptake level of NaHS@Cy5@MS@SP by RAW264.7 (**A**) and FLSs (**B**). (**C-D**) Represents fluorescence intensity statistics at different time points. *$P < 0.05$ versus RAW264.7. $n = 4–6$. NaHS, Sodium Hydrosulfide; MS, Mesoporous silicon; DIL, 1,1′-dioctadecyl-3,3,3′,3′-tetramethylindocarbocyanine perchlorate; SP, SP, Soy lecithin bimolecular polypeptide; FLSs, fibroblast-like synoviocytes

and NaHS significantly ameliorated LPS-induced inflammation. This was evidenced by a reduction in the release of IL-6 (Fig. 8D) and decreased mRNA levels of *IL-6* and *COX-2* (Fig. 8E-F). The observed reduction in *IL-6* and *COX-2* mRNA levels, along with decreased IL-6 release, underscores the efficacy of NaHS@Cy5@MS@SP in dampening inflammatory signaling pathways.

The CCK-8 assay (Fig. 8G) and EdU staining (Fig. 8H) confirmed that NaHS@Cy5@MS@SP and NaHS suppressed LPS-induced viability of FLSs. Additionally, NaHS@Cy5@MS@SP and NaHS treatment reduced the migratory capability of FLS cells, as demonstrated by the Boyden chamber assay (Fig. 8I-J). The inhibition of FLS cell viability and migration by NaHS@Cy5@MS@SP is particularly noteworthy, as these processes are critical in the progression of RA. Synoviocyte proliferation and migration contribute to the formation of pannus and joint destruction in RA, and their suppression by NaHS@Cy5@MS@SP highlights its therapeutic potential.

Moreover, treatment with NaHS@Cy5@MS@SP and NaHS led to decreased levels of vascular endothelial growth factor (VEGF) and reduced mRNA levels of matrix metalloproteinases (*MMP-1*, *MMP-3*, and *MMP-9*) in FLS cells (Fig. 8L). Importantly, the beneficial effects of NaHS@Cy5@MS@SP were more pronounced than those observed with NaHS treatment alone (Fig. 8). The reduction in VEGF levels and MMP expression by NaHS@Cy5@MS@SP points to its role in modulating angiogenesis and tissue remodeling, processes that are aberrantly regulated in RA. VEGF and MMPs facilitate the invasive and destructive behavior of synoviocytes, and their inhibition by NaHS@Cy5@MS@SP could prevent joint damage and disease progression. Notably, the effects of NaHS@Cy5@MS@SP were stronger than those of NaHS alone, suggesting that the formulation of NaHS

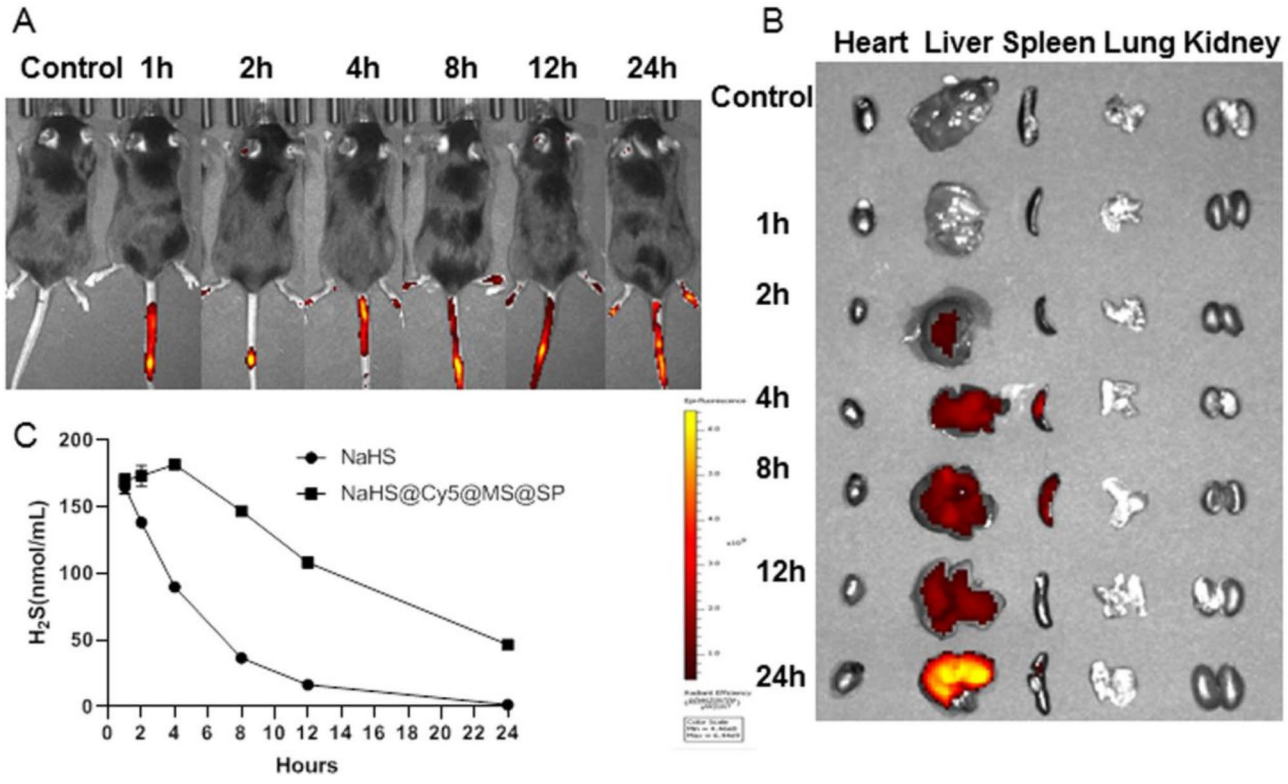

D

Treatments	C_{max}	$t_{1/2}$	AUC(nM)
NaHS	164.78	4.51±0.3	844±20.41
NaHS@Cy5@MS@SP	181.53	17.07±1.2	2649±28.81

Fig. 5 Biodistribution of NaHS@Cy5@MS@SP. (**A**) In vivo imaging of NaHS@Cy5@MS@SP, after 200 μL, 75 mg/kg NaHS@Cy5@MS@SP solution was injected into the tail vein of CIA mice for 1–24 h, fluorescence detection was performed at 650 nm. (**B**) Representative ex vivo images of NaHS@Cy5@MS@SP fluorescence of harvest organs (Heart, Liver, Spleen, Lung, Kidney) from CIA mice after different injection times. (**C**) NaHS circulation times in the serum of CIA mice after tail vein injection with NaHS (50 μm■kg^{-1}) and NaHS@Cy5@MS@SP (75 mg■kg^{-1}). Mean ± SEM. $n = 5$. (**D**) Pharmacokinetic parameters (C_{max}: maximum plasma concentration, $t_{1/2}$: elimination half-life and AUC_{inf}: area under the curve from zero to infinity). Mean ± SEM. $n = 5$

with Cy5 and MS@SP enhances its bioavailability or stability, leading to improved therapeutic outcomes. This enhanced efficacy warrants further investigation to fully understand the underlying mechanisms and to optimize the therapeutic potential of NaHS@Cy5@MS@SP for clinical application in RA. Overall, our findings indicate that NaHS@Cy5@MS@SP has potent anti-inflammatory effects in LPS-provoked FLS cells, making it a promising candidate for RA therapy. Future studies should focus on elucidating the detailed mechanisms of action and assessing the in vivo efficacy and safety of NaHS@Cy5@MS@SP in RA models.

NaHS@Cy5@MS@SP prevents the activation of the Hedgehog signaling pathway in FLSs

To elucidate the potential mechanism of H_2S in RA, we conducted transcriptome sequencing on FLSs exposed to LPS stimulation, with or without H_2S treatment. Following H_2S treatment, we identified 80 genes with elevated expression and 67 genes with decreased expression in LPS-stimulated FLSs (Fig. 9A-B). Gene set enrichment analysis (GSEA) revealed a significant positive correlation between H_2S treatment and the Hedgehog signaling pathway (Fig. 9C-D). Our transcriptome sequencing results highlight the significant impact of H_2S on gene expression in LPS-stimulated FLSs, revealing both upregulation and downregulation of numerous genes. These findings suggest a broad modulatory role of H_2S in inflammatory processes, with the potential to influence various pathways and cellular functions. The GSEA indicating a positive correlation between H_2S treatment and the Hedgehog signaling pathway is particularly intriguing. The Hedgehog pathway is known to play a crucial role in cell differentiation, proliferation, and tissue

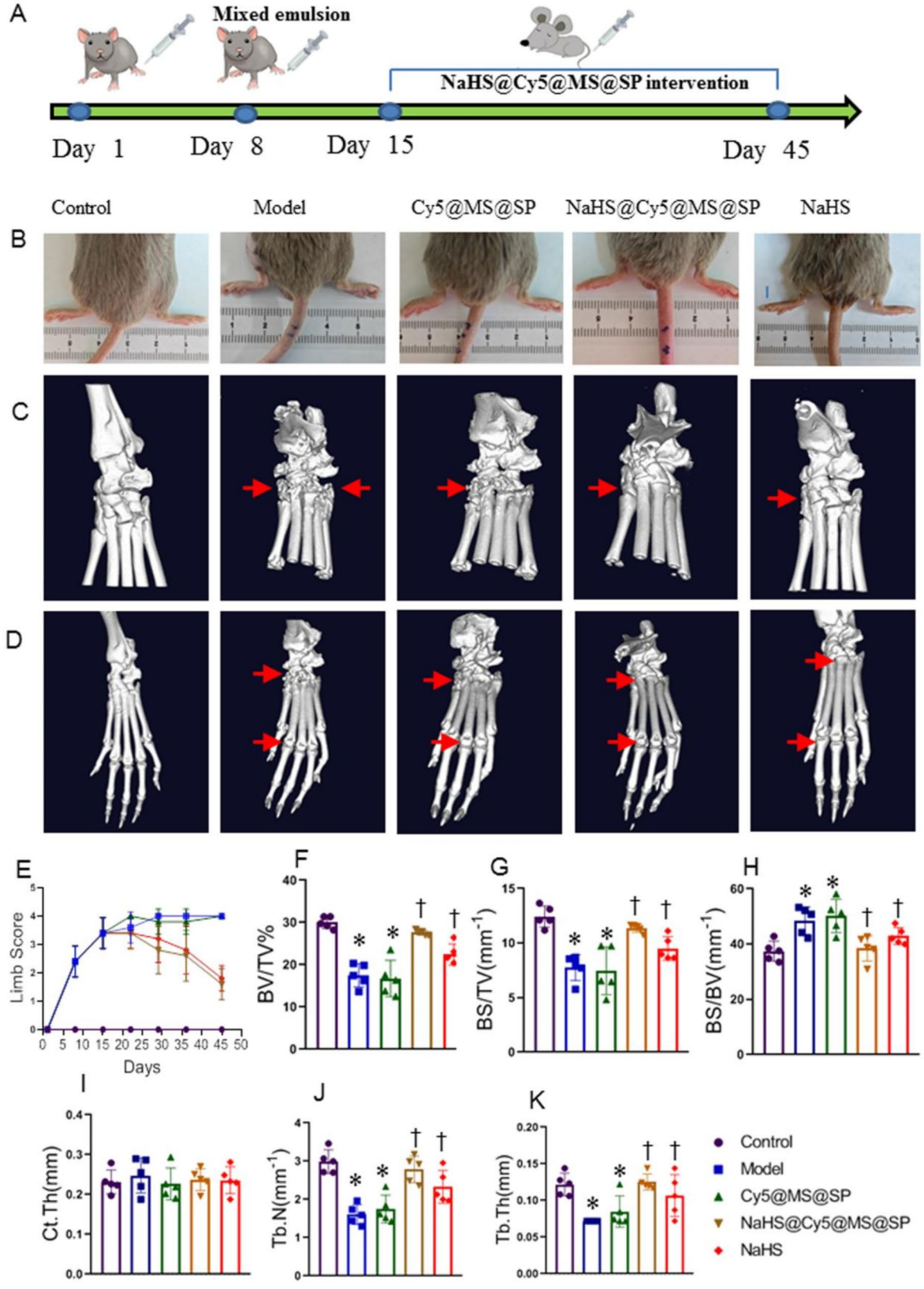

Fig. 6 Therapeutic effect of NaHS@Cy5@MS@SP on CIA mice. (**A**) Animal experiment design. (**B**) Photographs of the foot of CIA mice. (**C-D**) Micro-CT images of the ankle and foot of CIA mice. (**E**) Limb arthritis severity score. (**F-H**) BV/TV, BS/TV and BS/BV of CIA mice. (**I-K**) Ct.Th, Tb.N and Tb.Th of CIA mice. *$P < 0.05$ versus Control; †$P < 0.05$ versus Model. $n = 5$. BV, Bone volume; BS, Bone surface area; TV, Tissue volume; CIA, collagen-induced arthritis

(See figure on previous page.)

Fig. 7 Pathological staining of the knee joint was performed. (**A**) Representative images of Masson staining. (**B**) Representative images of Hematoxylin and eosin (HE) staining. (**C**) Representative images of Safranin fast green staining. (**D**) Representative IHC images of TNF-α in the joint site. (**E**) Representative IHC images of IL-6 IHC staining in the joint site. (**F** and **G**) Representative images of CD206 and CD86 staining in the synovium. (**H** and **I**) Quantitative analysis of TNF-α and IL-6 expression levels. (**J** and **K**) Quantitative analysis of CD206 and CD86 expression levels in synovium. *$P < 0.05$ versus Control; †$P < 0.05$ versus Model. $n = 6$. NaHS, Sodium Hydrosulfide; TNF-α, tumor necrosis factor-α. IL-6, interleukin-6

patterning [47]. Activation of this pathway contributes to disease progression by promoting FLS proliferation, inflammatory cytokine production, and joint destruction in RA [48]. Blocking Hedgehog signaling might decrease IL-6 production, which is a key cytokine in RA pathogenesis [11]. In RA, studies have shown increased expression of Hedgehog pathway-related proteins in synovial tissues compared to healthy controls [49, 50]. Further clinical trials are needed to explore Hedgehog inhibitors as adjunctive therapy in RA treatment.

To determine whether the Hedgehog signaling pathway is involved in the pathological process of RA, we used western blotting to analyze the protein expression levels of key pathway components: Sonic Hedgehog (SHH), Smoothened (SMO), and GLI family zinc finger 1 (GLI1). LPS stimulation resulted in increased protein levels of SHH, SMO, and GLI1, which were reversed by treatment with NaHS@Cy5@MS@SP and NaHS (Fig. 9E). Notably, NaHS@Cy5@MS@SP exhibited a stronger inhibitory effect compared to NaHS alone (Fig. 9).

The reversal of LPS-induced upregulation of SHH, SMO, and GLI1 by H_2S treatment suggests that H_2S exerts its anti-inflammatory effects, at least in part, by modulating the Hedgehog signaling pathway. The usage of western blotting to confirm the involvement of the Hedgehog pathway provides robust evidence supporting this mechanism. The findings that NaHS@Cy5@MS@SP had a stronger inhibitory effect on the protein levels of SHH, SMO, and GLI1 compared to NaHS alone underscore the enhanced efficacy of the nanocomposite formulation. This superior performance may be attributed to improved stability, targeted delivery, or increased bioavailability of H_2S when encapsulated in the NaHS@Cy5@MS@SP complex. The modulation of the Hedgehog pathway by H_2S adds a new dimension to our understanding of its therapeutic potential in RA. By inhibiting key components of this pathway, H_2S may help to reduce inflammation, prevent synovial hyperplasia, and inhibit the invasive behavior of FLS cells, all of which are hallmarks of RA pathology.

The effect of NaHS@Cy5@MS@SP on the Hedgehog signaling was abolished by SAG

SHH has been implicated in exacerbating articular injury and inflammation via the p38 mitogen-activated protein kinase (MAPK) signaling pathway [51]. To further verify the therapeutic effects of H_2S on RA in vitro, we investigated the impact of the Smoothened (SMO) agonist SAG on LPS-challenged FLSs treated with NaHS@Cy5@MS@SP and NaHS. Western blotting analysis revealed that SAG negated the inhibitory effects of NaHS@Cy5@MS@SP and NaHS on the protein expression levels of SHH, SMO, GLI1, and phosphorylated p38 (P-P38) (Fig. 10A). The reversal of the inhibitory effects on SHH, SMO, GLI1, and P-P38 by SAG indicates that the Hedgehog pathway is a key target of H_2S action in reducing inflammation and cell proliferation in RA. This is consistent with previous findings that SHH can exacerbate articular injury and inflammation through the p38 MAPK signaling pathway. Our data suggest that H_2S, via NaHS@Cy5@MS@SP and NaHS, mitigates these detrimental effects by downregulating this pathway.

Furthermore, SAG abolished the reductions in TNF-α and IL-6 levels induced by NaHS@Cy5@MS@SP and NaHS treatment (Fig. 10B). Similarly, RT-PCR analysis demonstrated that SAG markedly offset the suppressive effects of NaHS@Cy5@MS@SP and NaHS on the mRNA levels of *IL-6* and *COX2* (Fig. 10C). The abrogation of TNF-α and IL-6 reduction by SAG further highlights the role of the Hedgehog pathway in the inflammatory response. These cytokines are central mediators of inflammation in RA, and their regulation is crucial for controlling disease progression. The ability of SAG to counteract the suppression of IL-6 and COX2 mRNA levels by H_2S treatments provides additional evidence that H_2S exerts its anti-inflammatory effects through this pathway.

The decrease in cell viability and migration observed following NaHS@Cy5@MS@SP and NaHS treatment was reversed by SAG (Fig. 10D-F). The reversal of decreased cell viability and migration by SAG suggests that H_2S inhibits these processes through Hedgehog pathway modulation. This finding is significant, as synoviocyte proliferation and migration contribute to joint destruction and inflammation in RA. By targeting this pathway, H_2S treatments can potentially prevent these pathological processes.

Additionally, the suppression of VEGF release and the mRNA levels of matrix metalloproteinases (*MMP-1*, *MMP-3*, and *MMP-9*) by NaHS@Cy5@MS@SP and NaHS was dramatically reversed by SAG (Fig. 10G-H). The inhibition of VEGF release and MMP expression by H_2S, and the subsequent reversal by SAG, further corroborates the involvement of the Hedgehog pathway in angiogenesis and tissue remodeling in RA. VEGF and MMPs are key factors in these processes, and their

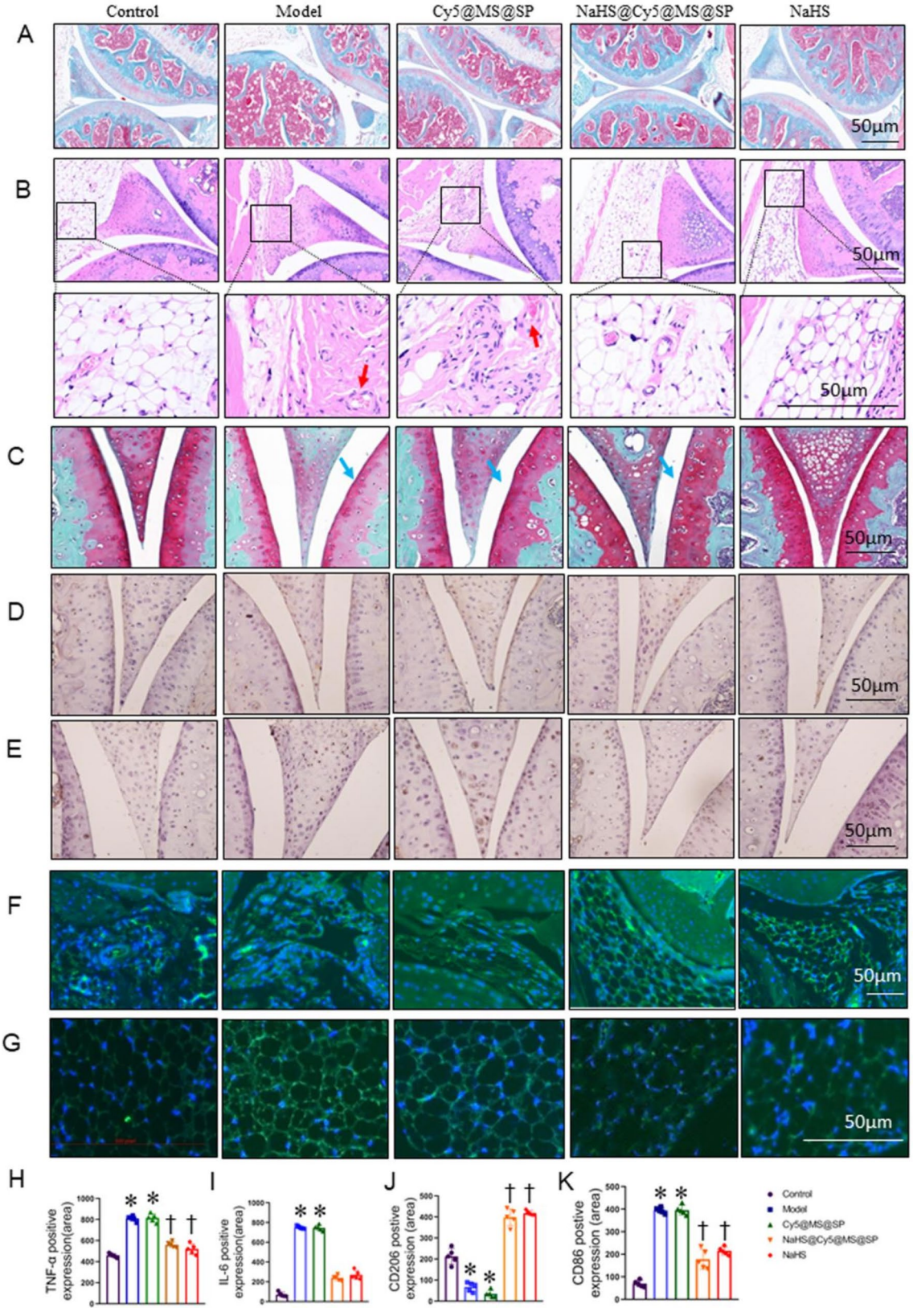

Fig. 7 (See legend on next page.)

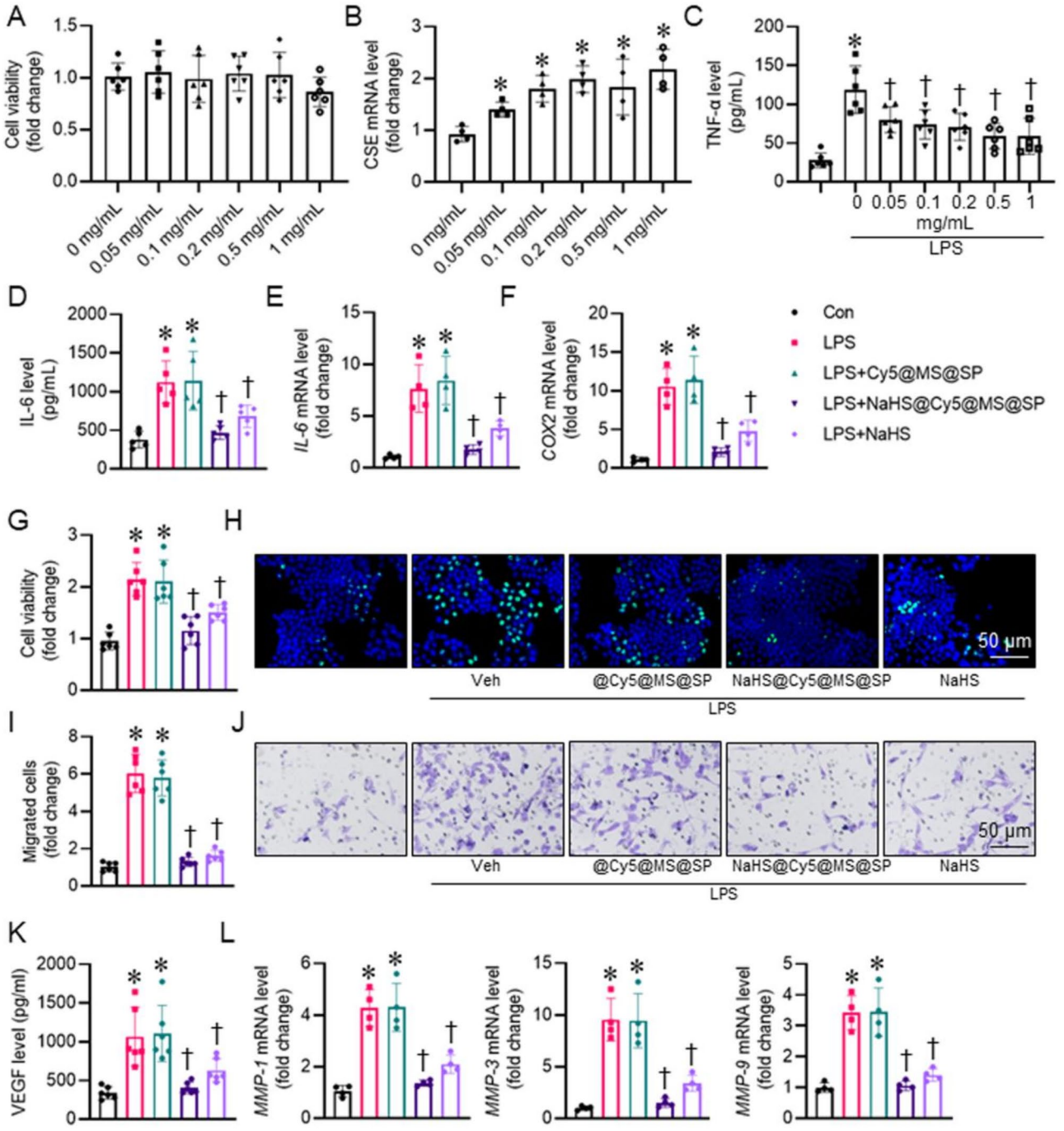

Fig. 8 NaHS@Cy5@MS@SP inhibited FLS cells inflammation and growth in vitro. (**A**) Effect of NaHS@Cy5@MS@SP on FLS viability. (**B**) RT-PCR analysis of CSE in FLSs treated with NaHS@Cy5@MS@SP. (**C**) ELISA analysis of TNF-α in FLSs treated with NaHS@Cy5@MS@SP. (**D**) The levels of IL-6 by ELISA. (**E-F**) RT-PCR analysis of *IL-6* and *COX2*. (**G**) Cell viability. (**H**) Representative photographs of EdU-positive cells. (**I-J**) Transwell migration assay. (**K**) The level of VEGF. (**L**) RT-PCR analysis of *MMP-1*, *MMP-3*, and *MMP-9*. *P < 0.05 versus Con; †P < 0.05 versus LPS. n = 4–6. NaHS, Sodium Hydrosulfide; FLSs, fibroblast-like synoviocytes; LPS, lipopolysaccharide; RT-PCR, Reverse transcription-polymerase chain reaction; IL-6, interleukin-6; COX2, cyclooxygenase-2; TNF-α, tumor necrosis factor-α; EdU, 5-Ethynyl-2′-deoxyuridine; VEGF, endothelial growth factor; MMP-1, matrix metalloproteinase-1; MMP-3, matrix metalloproteinase-3; MMP-9, matrix metalloproteinase-9

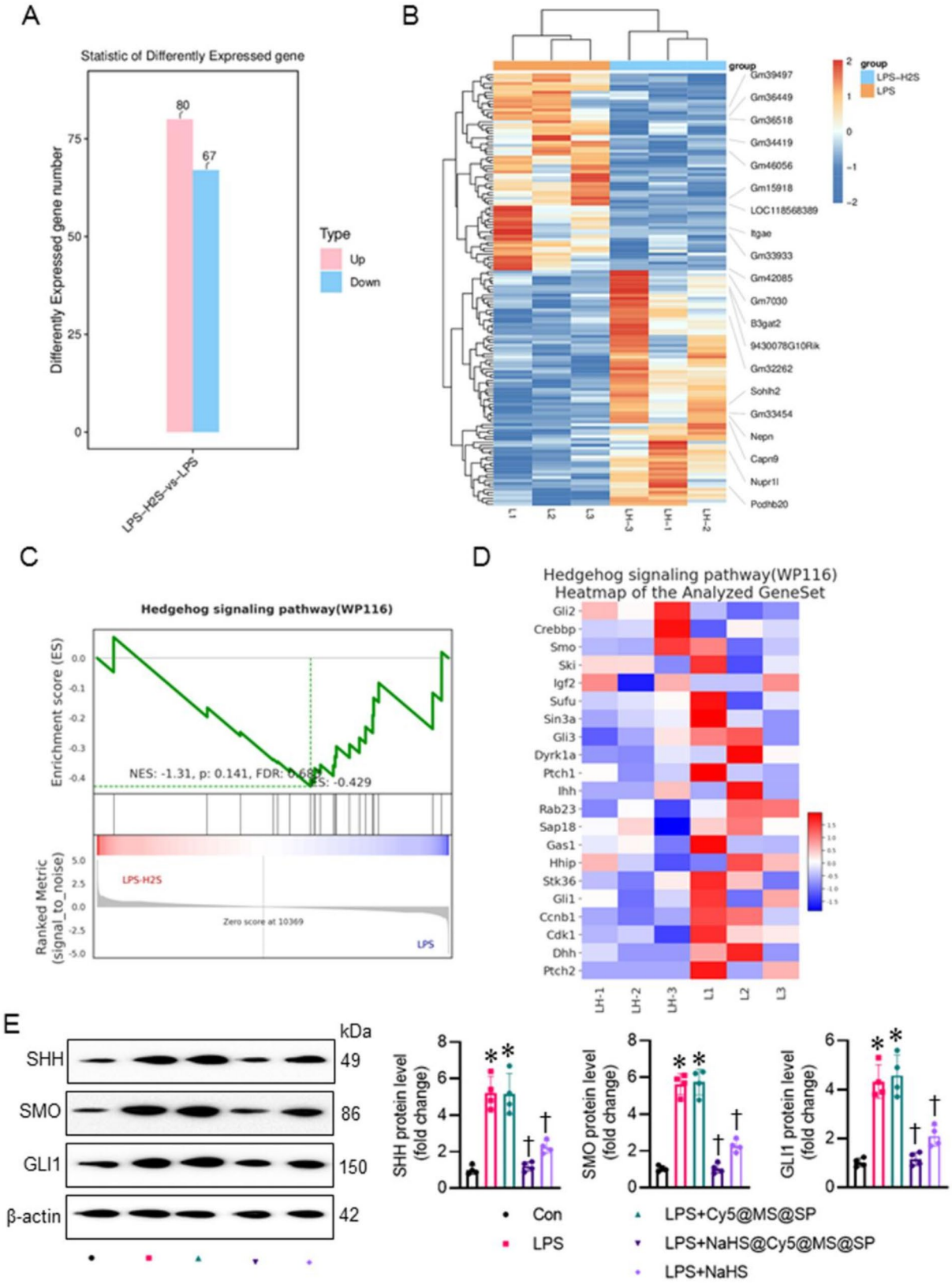

Fig. 9 (See legend on next page.)

(See figure on previous page.)

Fig. 9 NaHS@Cy5@MS@SP may inhibit FLS cells inflammation and growth via the Hedgehog signaling pathway. (**A**) The number of differentially expressed genes between LPS and LPS + H_2S group. (**B**) Heatmap of differentially expressed genes between LPS and LPS + H_2S group. (**C**) Gene set enrichment analysis of the Hedgehog signaling pathway. (**D**) Heatmap of the Analyzed GeneSet of the Hedgehog signaling pathway. (**E**) Western blot analysis of SHH, SMO, and GLI1 in FLS cells. *$P < 0.05$ versus Con; †$P < 0.05$ versus LPS. $n = 4$. NaHS, Sodium Hydrosulfide; H_2S, hydrogen sulfide; FLSs, fibroblast-like synoviocytes; LPS, lipopolysaccharide; SHH, Sonic Hedgehog; SMO, Smoothened; GLI1, GLI family zinc finger 1

regulation by H_2S indicates a broader therapeutic potential for H_2S in managing RA. Our study demonstrates that H_2S, particularly through NaHS@Cy5@MS@SP, exerts significant anti-inflammatory, anti-proliferative, and anti-migratory effects in LPS-challenged FLSs by modulating the Hedgehog signaling pathway. The reversal of these effects by the SMO agonist SAG underscores the critical role of this pathway in the therapeutic actions of H_2S. These findings provide a strong foundation for further research into H_2S-based therapies for RA, with a focus on targeting the Hedgehog pathway to achieve optimal therapeutic outcomes (Fig. 10).

Conclusion

In this study, we developed a dissolvable nanocomplex loaded with NaHS to achieve the stable and targeted release of H_2S in synoviocytes, resulting in the restored synovial homeostasis. Our results allowed NaHS@Cy5@MS@SP to alleviate inflammation and clinical symptoms in RA mice. Collectively, NaHS@Cy5@MS@SP might be a promising combinatorial anti-inflammatory strategy for preventing and treating RA by therapeutically targeting the Hedgehog signaling pathway in synoviocytes. The targeted Hedgehog pathway inhibitors or NaHS@Cy5@MS@SP may be developed for RA treatment, considering factors such as patient selection, biomarker identification, and potential combination therapies. The long-term efficacy studies and the potential clinical trial should be designed to assess the safety and therapeutic benefits of NaHS@Cy5@MS@SP in RA patients. Future studies are highly required to validate the efficacy and safety of NaHS@Cy5@MS@SP in human RA models, including clinical trials to assess its therapeutic potential in RA patients. Additionally, the potential applications of H_2S-releasing nanoparticles in other inflammatory diseases could be investigated, and the more targeted delivery systems, long-term stability, and dose optimization for clinical usage should be developed.

This cell type-specific uptake of NaHS@Cy5@MS@SP is a promising advantage for clinical and therapeutic applications. Notably, the cell type-specific uptake can vary significantly depending on cellular characteristics, which may influence therapeutic efficacy. Further studies are required to investigate uptake efficiency across different relevant cell types and provide quantitative data to clarify the selectivity of NaHS@Cy5@MS@SP. In addition, the potential factors influencing the cellular uptake of NaHS@Cy5@MS@SP, such as receptor expression and endocytosis mechanisms, will be explored in future studies. Moreover, the additional long-term data will be conducted to assess the sustained therapeutic effects of NaHS@Cy5@MS@SP on disease progression, inflammation, and joint protection in RA models in future studies. The particle stability and immune response of NaHS@Cy5@MS@SP were not directly assessed in this study. More studies are recommended to evaluate the potential barriers to translation, such as nanoparticle aggregation, degradation, or unintended immune activation of NaHS@Cy5@MS@SP in vivo. The particle clearance, biodistribution, and bioavailability of NaHS@Cy5@MS@SP should be considered, as these impact therapeutic efficacy and potential off-target effects. The standardized protocols are needed to assess the efficacy and long-term safety of NaHS@Cy5@MS@SP in diverse patient

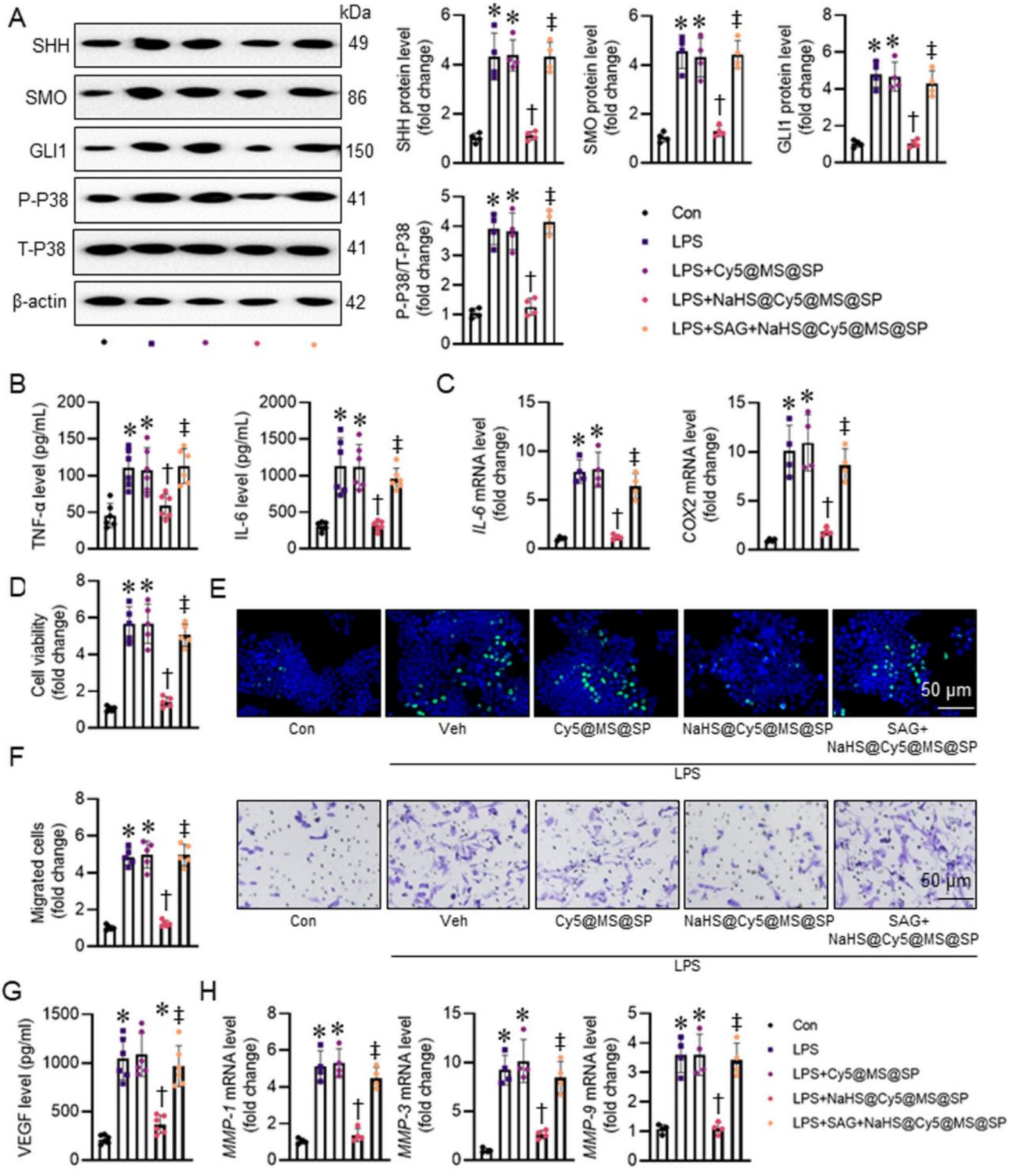

Fig. 10 SAG reversed the inhibitory effect of NaHS@Cy5@MS@SP on inflammation and cell growth in LPS-induced FLS cells. (**A**) Western blot analysis of SHH, SMO, GLI1, P-P38 and T-P38 protein levels in FLSs. (**B**) ELISA analysis of TNF-α and IL-6 in FLSs. (**C**) RT-PCR analysis of *IL-6* and *COX2*. (**D**) Cell viability. (**E**) Representative photographs of EdU-positive cells. (**F**) Transwell migration assay. (**G**) The level of VEGF. (**H**) RT-PCR analysis of *MMP-1*, *MMP-3*, and *MMP-9*. *P < 0.05 versus Con; †P < 0.05 versus LPS; ‡ P < 0.05 versus LPS + NaHS@Cy5@MS@SP. n = 4–6. NaHS, Sodium Hydrosulfide; H_2S, hydrogen sulfide; FLSs, fibroblast-like synoviocytes; LPS, lipopolysaccharide; SHH, Sonic Hedgehog; SMO, Smoothened; GLI1, GLI family zinc finger 1. LPS, lipopolysaccharide; RT-PCR, Reverse transcription-polymerase chain reaction; IL-6, interleukin-6; COX2, cyclooxygenase-2; TNF-α, tumor necrosis factor-α; EdU, 5-Ethynyl-2′-deoxyuridine; VEGF, endothelial growth factor; MMP-1, matrix metalloproteinase-1; MMP-3, matrix metalloproteinase-3; MMP-9, matrix metalloproteinase-9

populations. The variability in patient genetics, disease stage, and immune status of RA patients may impact therapeutic response of this nanoparticle.

Author contributions
Xue-Xue Zhu and An-Jing Xu: Data curation, Formal analysis, Investigation, Project administration, writing - original draft. Wei-Wei Cai and Shi-Jie Zhang: Investigation, Methodology, Visualization. Yuan-Yuan Wen, Xing-Yu Cao, Hao-Dong Li, Yue-Qing Du and You-Yi Zhuang: Investigation, Formal analysis. Jing Wang, Xiao-Ran Hu and Xin-Ran Bai: Software, Validation. Jia-Bao Su, Ao-Yuan Zhang, Qing-Bo Lu and Li-Ying Qiu: Investigation, Methodology, Software, Visualization. Zhi-Jun Han: Methodology, Visualization. Lin Pan, Bao Hou and Hai-Jian Sun: Conceptualization, Funding acquisition, Project administration, Resources, Writing - review & editing. All data were generated in-house, and no paper mill was used. All authors agree to be accountable for all aspects of work ensuring integrity and accuracy.

Funding
This work was funded and supported by the National Natural Science Foundation of China (82300414, 82370364 and 82170424), Jiangsu Province Excellent Youth Fund (BK20240204), Jiangsu Natural Science Foundation (BK20231049, BE2020634 and BK20191138), Basic Research Program of Jiangsu (BK20240477), Jiangsu Funding Program for Excellent Postdoctoral Talent (2024ZB844), the Fundamental Research Funds for the Central Universities (JUSRP124036), high-level introduction of talents and scientific research start-up funds of JNU (1286010241222100), Clinical Research and Translational Medicine Research Program of Affiliated Hospital of Jiangnan University (LCYJ202306, LCYJ202226), Wuxi Science and Technology Development Fund Project "Light of the Taihu Lake" (K20221028), Wuxi Municipal Health Commission Youth Project (Q202226), Wuxi Science and Technology Development Fund Project (Y20242106), Top Talent Support Program for young-aged people of Wuxi Health Committee (HB2023045), Medical Discipline Program of Wuxi Health Commission, the Science and Technology Projects of Wuxi City (M202207, BJ2023029).

Data availability
No datasets were generated or analysed during the current study.

Declarations

Ethics approval and consent to participate
The animal experimental ethics was approved by the Experimental Animal Ethics Committee of Jiangnan University (JN.No20230330d0400930[98]).

Consent for publication
All authors read and agreed to submit the manuscript.

Competing interests
The authors declare no competing interests.

Author details
[1]Department of Basic Medicine, Wuxi School of Medicine, Jiangnan University, Wuxi 214122, China
[2]Department of Clinical Research Center, Jiangnan University Medical Center, Wuxi 214001, China
[3]Department of Anesthesiology, Affiliated Hospital of Jiangnan University, Jiangnan University, Wuxi 214122, China
[4]Department of Endocrinology, Affiliated Hospital of Jiangnan University, Jiangnan University, Wuxi 214122, China
[5]Department of Orthopedics, Central Laboratory, Changshu Hospital Affiliated to Soochow University, First People's Hospital of Changshu City, Changshu 215506, China
[6]Key Laboratory of Multifunctional Nanomaterials and Smart Systems, Suzhou Institute of Nano-Tech and Nano-Bionics, Chinese Academy of Sciences, Suzhou 215123, China
[7]State Key Laboratory of Natural Medicines, China Pharmaceutical University, No. 24 Tongjia Lane, Nanjing 210009, China

Received: 28 November 2024 / Accepted: 2 March 2025
Published online: 08 March 2025

References

1. Tan CY, Wong JX, Chan PS, Tan H, Liao D, Chen W, et al. Yin Yang 1 suppresses dilated cardiomyopathy and cardiac fibrosis through regulation of bmp7 and Ctgf. Circ Res. 2019;125:834–46.
2. Deng Y, Zheng H, Li B, Huang F, Qiu Y, Yang Y, et al. Nanomedicines targeting activated immune cells and effector cells for rheumatoid arthritis treatment. J Control Release. 2024;371:498–515.
3. Finckh A, Gilbert B, Hodkinson B, Bae SC, Thomas R, Deane KD, et al. Global epidemiology of rheumatoid arthritis. Nat Rev Rheumatol. 2022;18:591–602.
4. Radu AF, Bungau SG. Management of rheumatoid arthritis: an overview. Cells 2021;10.
5. Shen Q, Du Y. A comprehensive review of advanced drug delivery systems for the treatment of rheumatoid arthritis. Int J Pharm. 2023;635:122698.
6. Nygaard G, Firestein GS. Restoring synovial homeostasis in rheumatoid arthritis by targeting fibroblast-like synoviocytes. Nat Rev Rheumatol. 2020;16:316–33.
7. Alivernini S, Macdonald L, Elmesmari A, Finlay S, Tolusso B, Gigante MR, et al. Distinct synovial tissue macrophage subsets regulate inflammation and remission in rheumatoid arthritis. Nat Med. 2020;26:1295–306.
8. Hua P, Liang R, Yang S, Tu Y, Chen M. Microneedle-assisted dual delivery of puma gene and Celastrol for synergistic therapy of rheumatoid arthritis through restoring synovial homeostasis. Bioact Mater. 2024;36:83–95.
9. Croft AP, Campos J, Jansen K, Turner JD, Marshall J, Attar M, et al. Distinct fibroblast subsets drive inflammation and damage in arthritis. Nature. 2019;570:246–51.
10. Lu Q, Jiang Y, Cang X, Pan J, Shen X, Tang R et al. Study of the immune infiltration and Sonic Hedgehog expression mechanism in synovial tissue of rheumatoid arthritis-related interstitial lung disease under machine learning Cibersort algorithm. Mol Biotechnol 2024.
11. Li P, Huang Y, Wang J, Zeng J, Li L. Platycodin d relieves rheumatoid arthritis by promoting apoptosis of mitochondria to inhibit activation of Hedgehog pathway. Autoimmunity. 2023;56:2205053.
12. Lin L, Zhu S, Huang H, Wu LP, Huang J. Chemically modified small interfering Rna targeting Hedgehog signaling pathway for rheumatoid arthritis therapy. Mol Ther Nucleic Acids. 2023;31:88–104.
13. Qin S, Sun D, Li H, Li X, Pan W, Yan C, et al. The effect of shh-gli signaling pathway on the synovial fibroblast proliferation in rheumatoid arthritis. Inflammation. 2016;39:503–12.
14. Wang M, Zhu S, Peng W, Li Q, Li Z, Luo M, et al. Sonic Hedgehog signaling drives proliferation of synoviocytes in rheumatoid arthritis: a possible novel therapeutic target. J Immunol Res. 2014;2014:401903.
15. Sun HJ, Wu ZY, Nie XW, Bian JS. Role of endothelial dysfunction in cardiovascular diseases: the link between inflammation and hydrogen sulfide. Front Pharmacol. 2019;10:1568.
16. Lu QB, Fu X, Liu Y, Wang ZC, Liu SY, Li YC, et al. Disrupted cardiac fibroblast Bcaa catabolism contributes to diabetic cardiomyopathy via a periostin/nap1l2/sirt3 axis. Cell Mol Biol Lett. 2023;28:93.
17. Sun HJ, Lu QB, Zhu XX, Ni ZR, Su JB, Fu X, et al. Pharmacology of hydrogen sulfide and its donors in cardiometabolic diseases. Pharmacol Rev. 2024;76:846–95.
18. Sun HJ, Wu ZY, Cao L, Zhu MY, Liu TT, Guo L et al. Hydrogen sulfide: recent progression and perspectives for the treatment of diabetic nephropathy. Molecules 2019;24.
19. Sun HJ, Wu ZY, Nie XW, Wang XY, Bian JS. An updated insight into molecular mechanism of hydrogen sulfide in cardiomyopathy and myocardial ischemia/reperfusion injury under diabetes. Front Pharmacol. 2021;12:651884.
20. Whiteman M, Haigh R, Tarr JM, Gooding KM, Shore AC, Winyard PG. Detection of hydrogen sulfide in plasma and knee-joint synovial fluid from rheumatoid arthritis patients: relation to clinical and laboratory measures of inflammation. Ann N Y Acad Sci. 2010;1203:146–50.
21. Li M, Hu W, Wang R, Li Z, Yu Y, Zhuo Y et al. Sp1 s-sulfhydration induced by hydrogen sulfide inhibits inflammation via hdac6/myd88/nf-kappab signaling pathway in adjuvant-induced arthritis. Antioxid (Basel) 2022;11.
22. Wu WJ, Jia WW, Liu XH, Pan LL, Zhang QY, Yang D, et al. S-propargyl-cysteine attenuates inflammatory response in rheumatoid arthritis by modulating the nrf2-are signaling pathway. Redox Biol. 2016;10:157–67.

23. Kloesch B, Liszt M, Broell J. H2s transiently blocks il-6 expression in rheumatoid arthritic fibroblast-like synoviocytes and deactivates p44/42 mitogen-activated protein kinase. Cell Biol Int. 2010;34:477–84.
24. Wu W, Qin M, Jia W, Huang Z, Li Z, Yang D, et al. Cystathionine-gamma-lyase ameliorates the histone demethylase jmjd3-mediated autoimmune response in rheumatoid arthritis. Cell Mol Immunol. 2019;16:694–705.
25. Geng W, Liu X, Tao B, He Y, Li K, Gao P, et al. Nitric oxide scavenging and hydrogen sulfide production synergistically treat rheumatoid arthritis. Adv Healthc Mater. 2023;12:e2202380.
26. Zhao J, Bian E, Zhang R, Xu T, Nie Y, Wang L, et al. Self-assembled aza-boron-dipyrromethene-based h(2)s prodrug for synergistic ferroptosis-enabled gas and sonodynamic tumor therapies. Adv Sci (Weinh). 2024;11:e2309542.
27. Hao F, Lee RJ, Zhong L, Dong S, Yang C, Teng L, et al. Hybrid micelles containing methotrexate-conjugated polymer and co-loaded with microrna-124 for rheumatoid arthritis therapy. Theranostics. 2019;9:5282–97.
28. Zheng X, Yang H, Zhang Z, Liang X, Liu Y, Wang C, et al. Ph-responsive size-adjustable liposomes induce apoptosis of fibroblasts and macrophages for rheumatoid arthritis treatment. Acta Biomater. 2024;179:256–71.
29. Cerda MM, Zhao Y, Pluth MD. Thionoesters: a native chemical ligation-inspired approach to cysteine-triggered h(2)s donors. J Am Chem Soc. 2018;140:12574–9.
30. Yu Y, Wang Z, Ding Q, Yu X, Yang Q, Wang R et al. The Preparation of a novel poly(lactic acid)-based sustained h(2)s releasing microsphere for rheumatoid arthritis alleviation. Pharmaceutics 2021;13.
31. Wang X, Huang X, Zhang Y, Huo H, Zhou G, Shen L, et al. Hydrogen sulfide attenuates disturbed flow-induced vascular remodeling by inhibiting ldhb-mediated autophagic flux. Redox Biol. 2025;79:103456.
32. Hou B, Cai W, Zhang S, Xu A, Wen Y, Wang Y et al. Sustained-release h(2)s nanospheres regulate the inflammatory microenvironment of wounds, promote angiogenesis and collagen deposition, and accelerate diabetic wound healing. ACS Appl Bio Mater 2025.
33. Feng X, Gao G, Yu C, Zhu A, Chen J, Chen K, et al. Transcriptome and metabolome analysis reveals anthocyanin biosynthesis pathway associated with Ramie (boehmeria Nivea (l.) Gaud.) leaf color formation. BMC Genomics. 2021;22:684.
34. Sun HJ, Tan JX, Shan XD, Wang ZC, Wu ZY, Bian JS, et al. Dr region of nkaalpha1 is a target to ameliorate hepatic lipid metabolism disturbance in obese mice. Metabolism. 2023;145:155579.
35. Perna AF, Sepe I, Lanza D, Capasso R, Zappavigna S, Capasso G, et al. Hydrogen sulfide reduces cell adhesion and relevant inflammatory triggering by preventing adam17-dependent tnf-alpha activation. J Cell Biochem. 2013;114:1536–48.
36. Han X, Wang L, Shang Y, Liu X, Yuan J, Shen J. Hydrogen sulfide-releasing polyurethane/gelatin/keratin-ta conjugate Mats for wound healing. J Mater Chem B. 2022;10:8672–83.
37. Antoniadou I, Georgiou M, Dotsikas Y, Lamprou A, Lougiakis N, Pouli N, et al. Novel h(2)s-releasing bifunctional antihistamine molecules with improved antipruritic and reduced sedative actions. J Med Chem. 2023;66:9607–21.
38. Shen D, Yang J, Li X, Zhou L, Zhang R, Li W, et al. Biphase stratification approach to three-dimensional dendritic biodegradable mesoporous silica nanospheres. Nano Lett. 2014;14:923–32.
39. Tan H, Song Y, Chen J, Zhang N, Wang Q, Li Q, et al. Platelet-like fusogenic liposome-mediated targeting delivery of mir-21 improves myocardial remodeling by reprogramming macrophages post myocardial ischemia-reperfusion injury. Adv Sci (Weinh). 2021;8:e2100787.
40. Clayton PM, Vas CA, Bui TT, Drake AF, Mcadam K. Spectroscopic studies on nicotine and Nornicotine in the Uv region. Chirality. 2013;25:288–93.
41. Mishra KK, Borish K, Singh G, Panwaria P, Metya S, Madhusudhan MS, et al. Observation of an unusually large Ir red-shift in an unconventional s-h… S hydrogen-bond. J Phys Chem Lett. 2021;12:1228–35.
42. Antill AC, Ballard DH, Hollister AM, Rogers EJ, Yang S, Lokitz SJ. Micro-ct evaluation of rheumatoid arthritis mouse model disease progression: manual tracings versus semi-automated routines. Diagn Interv Imaging. 2016;97:651–5.
43. Song Y, Zhu F, Lin F, Zhang F, Zhang S. Bone quality, and the combination and penetration of cement-bone interface: a comparative micro-ct study of osteoarthritis and rheumatoid arthritis. Med (Baltim). 2018;97:e11987.
44. Mochizuki T, Yano K, Ikari K, Hiroshima R, Ishibashi M, Okazaki K. Change of Arashi scores for large joints in rheumatoid arthritis patients treated with abatacept for three years: a clinical observational study. Arch Rheumatol. 2021;36:10–8.
45. Li B, Guo Z, Qu J, Zhan Y, Shen Z, Lei X. The value of different involvement patterns of the knee synovio-entheseal complex in the differential diagnosis of spondyloarthritis, rheumatoid arthritis, and osteoarthritis: an mri-based study. Eur Radiol. 2023;33:3178–87.
46. Shan Z, Bi H, Suonan A, Gu Y, Zhou H, Xi K, et al. Tobacco mosaic viral nanoparticle inhibited osteoclastogenesis through inhibiting Mtor/akt signaling. Int J Nanomed. 2020;15:7143–53.
47. Yoshida S, Yoshida K. Regulatory mechanisms governing Gli proteins in Hedgehog signaling. Anat Sci Int. 2025;100:143–54.
48. Cai L, Meng B, Jiang F, Shu WH, Wang XH, Wang MQ, et al. Novel hif-1alpha inhibitor amsp-30m mitigates the pathogenic cellular behaviors of hypoxia-stimulated fibroblast-like synoviocytes and alleviates collagen-induced arthritis in rats via inhibiting Sonic Hedgehog pathway. Inflammation. 2023;46:2289–305.
49. Zhu S, Ye Y, Shi Y, Dang J, Feng X, Chen Y, et al. Sonic Hedgehog regulates proliferation, migration and invasion of synoviocytes in rheumatoid arthritis via Jnk signaling. Front Immunol. 2020;11:1300.
50. Al-Azab M, Wei J, Ouyang X, Elkhider A, Walana W, Sun X, et al. Tl1a mediates fibroblast-like synoviocytes migration and Indian Hedgehog signaling pathway via tnfr2 in patients with rheumatoid arthritis. Eur Cytokine Netw. 2018;29:27–35.
51. Zhu S, Dang J, Shi Y, Feng X, Hu Y, Lin L, et al. Sonic Hedgehog promotes synovial inflammation and articular damage through p38 mitogen-activated protein kinase signaling in experimental arthritis. J Autoimmun. 2022;132:102902.

Publisher's note